Deep-Sea Research II 56 (2009) 1164–1181

Contents lists available at ScienceDirect

Deep-Sea Research II

journal homepage: www.elsevier.com/locate/dsr2

The western Arctic boundary current at 152°W: Structure, variability, and transport

Anna Nikolopoulos [a,*], Robert S. Pickart [a], Paula S. Fratantoni [a], Koji Shimada [b], Daniel J. Torres [a], E. Peter Jones [c]

[a] Woods Hole Oceanographic Institution, Woods Hole, MA 02543, USA
[b] Institute of Observational Research for Global Change, Japan Agency for Marine-Earth Science and Technology, Yokosuka 237-0061, Japan
[c] Bedford Institute of Oceanography, Dartmouth, Nova Scotia, B2Y 4A3, Canada

ARTICLE INFO

Article history:
Accepted 27 October 2008
Available online 11 November 2008

Keywords:
Polar oceanography
Shelf-edge dynamics
Boundary currents
Volume transport
Pacific water
Atlantic water

ABSTRACT

From August 2002 to September 2004 a high-resolution mooring array was maintained across the western Arctic boundary current in the Beaufort Sea north of Alaska. The array consisted of profiling instrumentation, providing a timeseries of vertical sections of the current. Here we present the first-year velocity measurements, with emphasis on the Pacific water component of the current. The mean flow is characterized as a bottom-intensified jet of O (15 cm s^{-1}) directed to the east, trapped to the shelfbreak near 100 m depth. Its width scale is only 10–15 km. Seasonally the flow has distinct configurations. During summer it becomes surface-intensified as it advects buoyant Alaskan Coastal water. In fall and winter the current often reverses (flows westward) under upwelling-favorable winds. Between the storms, as the eastward flow re-establishes, the current develops a deep extension to depths exceeding 700 m. In spring the bottom-trapped flow advects winter-transformed Pacific water emanating from the Chukchi Sea. The year-long mean volume transport of Pacific water is 0.13 ± 0.08 Sv to the east, which is less than 20% of the long-term mean Bering Strait inflow. This implies that most of the Pacific water entering the Arctic goes elsewhere, contrary to expected dynamics and previous modeling results. Possible reasons for this are discussed. The mean Atlantic water transport (to 800 m depth) is 0.047 ± 0.026 Sv, also smaller than anticipated.

1. Introduction

It is generally believed that the halocline of the interior Arctic Ocean is ventilated through lateral processes (Aagaard and Carmack, 1994). In the Canada Basin, the cold halocline source waters of Pacific origin are made saline and dense in wintertime through cooling and brine rejection on the Bering/Chukchi shelves (e.g., Muench et al., 1988; Weingartner et al., 1998). The precise means by which these waters then enter the interior basin remains unclear, however. Shelf-basin exchange is believed to take place through a variety of mechanisms. These include dense water plumes through canyons (Garrison and Becker, 1976), cross-stream wind-forced flow (Melling, 1993), and eddy formation (Manley and Hunkins, 1985). Direct evidence of such exchange, however, is largely lacking. Most of the mechanisms seem to involve, in one way or another, the presence of a boundary current along the edge of the shelf.

The first measurements of the subsurface circulation along the shelf edge and slope of the southern Canada Basin were made by Aagaard (1984). He observed a bathymetrically steered eastward flow, named the Beaufort Undercurrent, seaward of the 50 m isobath (northern edge unknown) between 146° and 152°W. Geostrophic shear calculations, in agreement with velocity observations, indicated an increased flow with depth down to at least 600 m. Aagaard (1984) postulated that the undercurrent extended from 50 m to as deep as 2500 m over a horizontal distance of 60–70 km, hence transporting Bering Sea, Chukchi Sea, and Atlantic water masses. In a later investigation Aagaard (1989) presented current measurements from two depths on the slope near 147°W, supporting the idea of an eastward current with its core located over the outer shelf. The flow was found to be negligible at 1000 m depth, but due to the coarse resolution of the current meters the precise location of the maximum and the vertical extent of the current could not be determined. Recently, Pickart (2004) investigated the circulation along the Alaskan Beaufort Sea shelf edge using historical hydrographic and current meter data collected between 1950 and 1987. Individual hydrographic cross-sections were combined to produce a section of mean geostrophic velocity, which was then referenced with the

* Corresponding author: Currently at AquaBiota Water Research AB, Svante Arrhenius väg 21A, SE-104 05 Stockholm, Sweden. Tel.: +46 8 161012.
E-mail address: anna.nikolopoulos@aquabiota.se (A. Nikolopoulos).

0967-0645/$ - see front matter © 2008 Published by Elsevier Ltd.
doi:10.1016/j.dsr2.2008.10.014

mean current meter data. This indicated the presence of a narrow (order 20 km) eastward current centered between 150 and 200 m depth. Pickart (2004) referred to this as the Beaufort shelfbreak jet. It was found to have three distinct seasonal configurations and to transport a significant fraction of the Bering Strait inflow.

Farther to the west, along the Chukchi Sea shelfbreak and slope, there is also evidence for an eastward-flowing boundary current. Although no mean sections have been constructed, individual synoptic sections of absolute geostrophic velocity (under light to moderate winds) indicate the presence of a shelfbreak jet with a similar structure to that in the Beaufort Sea (Mathis et al., 2007; Llinas et al., 2008). What is the source of the shelfbreak current along the Chukchi and Beaufort Seas? Models suggest that the northward flow of Pacific water emanating from Bering Strait should turn eastward upon reaching the Chukchi shelf edge to form such a current (Winsor and Chapman, 2004; Spall, 2007). Observations indicate a strong flow of Pacific-origin water through Herald Canyon on the western Chukchi shelf (Woodgate et al., 2005a; Pickart, 2009a) and through Barrow Canyon on the eastern shelf (Münchow and Carmack, 1997; Pickart et al., 2005). A third branch of Pacific water on the shelf is believed to exist through the gap between Herald and Hanna Shoals, known as the Central Channel (Woodgate et al., 2005a; Weingartner et al., 2005; Fig. 1). Presumably, these branches feed the current along the shelf edge of the Chukchi/Beaufort Seas.

Synoptically, the shelfbreak current can reverse and flow to the west (e.g., Münchow et al., 2006), likely in response to wind forcing (Pickart et al., 2006). Also, distributions of Pacific-origin summer waters in the western Arctic suggest a northward pathway from the Chukchi shelf into the western part of the Beaufort gyre and the transpolar drift (Shimada et al., 2001; Steele et al., 2004). This is consistent with newly collected current meter data on the upper Chukchi slope near 166°W, which reveals northward directed currents over significant periods of time (R. Woodgate and K. Aagaard, pers. comm., 2007). In general, though, the impression one gets from the locus of shipboard and mooring data is that of an eastward-flowing boundary current along the edge of the southern Canada Basin. However, the paucity of the data collected in the vicinity of the shelfbreak up until now has prohibited determination of the detailed structure and dynamical characteristics of the current.

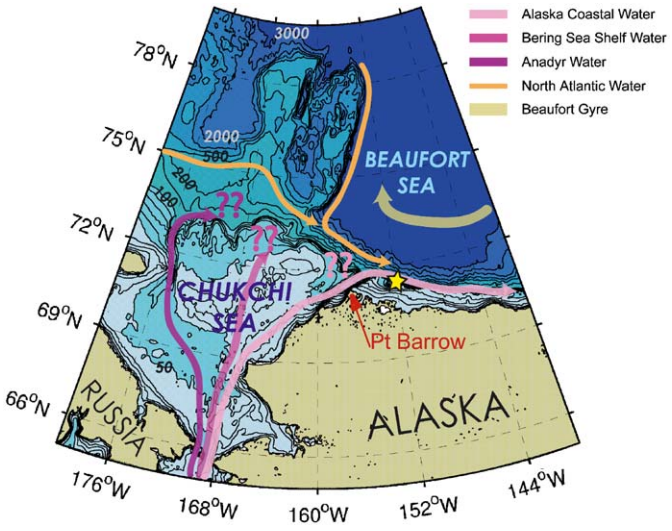

Fig. 1. Bathymetric map of the Chukchi Sea and parts of the Beaufort Sea and shelf; depths in m. The arrows show schematic pathways of the Pacific water inflow, the surface Beaufort Gyre, and the deeper boundary current of Atlantic water (that travels cyclonically around the boundaries of the Arctic basins). The star marks the site of the high-resolution mooring array. The weather station whose wind data are used in the study is located at Pt. Barrow.

As part of the Western Arctic Shelf-Basin Interactions (SBI) experiment, a high-resolution mooring array was deployed across the Beaufort shelf and slope, downstream of the Chukchi shelf outflows (Fig. 1). The array measured velocity, temperature and salinity and was deployed in August 2002 for two years (with a turnaround after one year). The aim of the multidisciplinary SBI project was to understand the fate of the Pacific-origin water in the Western Arctic, and the impact of this water on the ventilation of the interior basin, from a physical as well as biogeochemical perspective (Grebmeier and Harvey, 2005). The SBI study domain extended from Bering Strait to the Chukchi slope (within US territory) and to the Beaufort shelf and slope (to approximately 152°W; Fig. 1).

In this paper we analyze the velocity measurements from the first deployment-year of the Beaufort slope mooring array. The array has provided the first-ever high-resolution view of an Arctic boundary current and thus presents the opportunity to address a host of scientific questions. Our study focuses on the circulation of Pacific-origin waters and is hence mainly limited to the upper 300 m of the water column.

2. Data and methods

In August 2002, eight moorings (BS1–8) were deployed across the Beaufort shelfbreak and continental slope at 152°W (Fig. 1). The array spanned a total distance of about 40 km between the 50 and 1400-m isobaths, with a horizontal spacing of 4–6 km between the shallower moorings and 11 km between the two offshore-most sites (Fig. 2). The array consisted mostly of profiling instruments for measuring the velocity and hydrography. All of the moorings except the shallowest (BS1) were equipped with conductivity/temperature/depth (CTD) profilers providing vertical traces of temperature and salinity 2–4 times daily. Sites BS2–6 contained coastal moored profilers (Fratantoni et al., 2006) and BS7–8 consisted of McLane moored profilers (Doherty et al., 1999). At BS1 the hydrographic measurements were made by a bottom-mounted Seacat. As mentioned above, the focus of this paper is on the characteristics of the boundary current velocity field, and for the most part we use the current meter data. However, some aspects of the hydrography are presented to help in the overall analysis and interpretation. The reader is referred to Fratantoni et al. (2006) and Spall et al. (2008) for discussions of the accuracy of the temperature and salinity data. Overall, the CTD temperature was accurate to 0.002 °C and the salinity to 0.03.

For measuring velocity, upward-looking acoustic Doppler current profilers (ADCPs) were situated at the base of moorings BS1–6. The three shallowest sites had RDI Workhorse instruments (300 KHz), and the three deeper sites had RDI Longrangers (75 KHz). Since the locations of BS7 and 8 were too deep to use ADCPs, the moored profilers were equipped with three-axis acoustic travel-time current meters (ACMs). Velocity profiles were obtained once an hour at the ADCP sites and twice daily (at 0 and 6 GMT) at the ACM sites. For the bin size and ensemble averaging used here, the ADCP instrument uncertainty is $\pm 0.5\,\mathrm{cm\,s^{-1}}$. The ACM uncertainty is estimated to be $\pm 2\,\mathrm{cm\,s^{-1}}$ (see Våge et al., 2008).

Due to the different instruments and settings used, the vertical resolution and range of the velocity measurements varied across the array (Fig. 2). All instruments were recovered during the turnaround in September 2003 and overall the data return was very good. However, some data shortfall was experienced at a couple of the mooring sites. The BS1 tripod was accidentally deployed sideways and hence returned no good velocity data, and

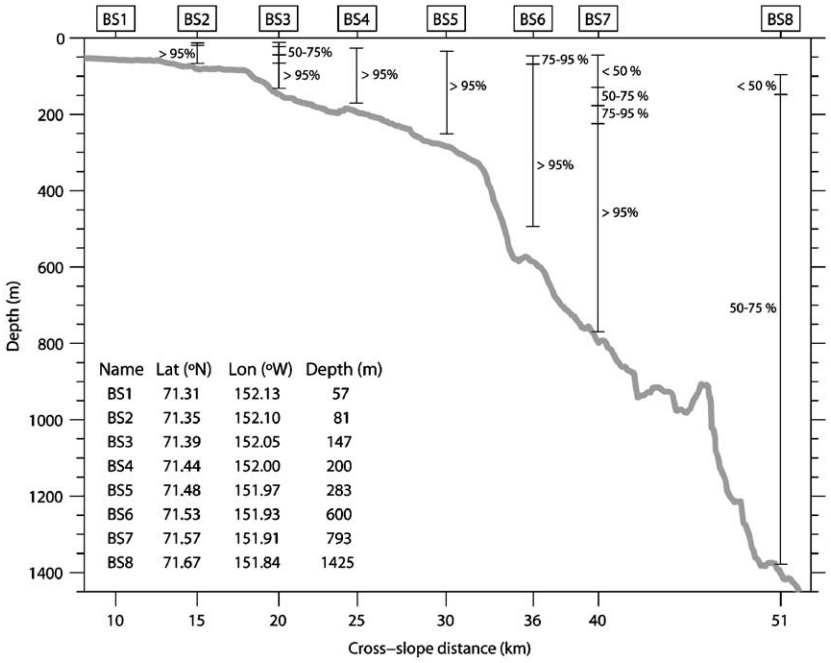

Fig. 2. Configuration of the Beaufort-slope mooring array in relation to the bottom topography. The mooring names are indicated at the top (coordinates and depths given in the table). The moorings were separated by 4–6 km (11 km for BS8), according to the horizontal-axis tick marks. Vertical lines show the data depth-range, and percentages indicate the temporal coverage of data, in relation to the full record length of August 2, 2002–July 31, 2003 (BS8 failed in March 2003, hence the reduced percentages throughout the depth range of this mooring). The data were averaged into depth bins that were 5 m thick at BS2–3, 10 m at BS4–6 and 2 m at BS7–8, respectively. The cross-slope distance is measured relative to the shoreward-most CTD station occupied during the SBI program and not the distance from the coast (BS1 is located approximately 50 km from the Alaskan coast).

the BS8 ACM failed in March 2003, four months prior to the turnaround. Fortunately, these two data gaps occurred at the edges of the mooring array, away from the core of the boundary current. At a few of the interior mooring sites the upper bins experienced some data deficit (Fig. 2). In the case of BS3 we believe that the absence of biological scatterers was the cause of this, resulting in sparse coverage in the upper 60 m between November and May. In the case of BS7, the profiler was unable to consistently reach the top of its profiling range, from November onward.

To carry out our analysis the velocity data were objectively gridded onto regularly spaced vertical sections. Prior to constructing these sections, temporal gaps spanning less than 6 h were linearly interpolated in time in the original timeseries. The timeseries were subsequently low-passed using a second-order Butterworth filter with a 36-h cut-off period, and subsampled once per day at 0 GMT. Typically, the Beaufort shelf is associated with low tidal energy levels; the amplitudes of the four dominant tidal constituents (O1, Q1, M2, and S2) were computed and found to be less than 1.5 cm s^{-1}. Nevertheless, the low-pass filter was applied to remove the effect of tides and inertial oscillations, since the focus of this study is on mesoscale to seasonal processes. We defined a rotated coordinate system aligned with the dominant direction of the core of the flow. This was guided by both the mean depth-averaged vectors and the orientation of the principle axis variance ellipses. The alongstream direction of the rotated system is 125°T (Fig. 3). The rotated velocity data were gridded using Laplacian-spline interpolation (tension factor of 5) onto daily vertical cross-sections with a horizontal grid spacing of 2 km and vertical grid spacing of 5 m. The sections were extrapolated to the surface and to the bottom (using the same 2-D Laplacian-spline scheme). Within the domain between 14–40 km and 0–300 m (as shown, for example, in Fig. 4), the extrapolated data occupy 10–30% of the total section area (on average 17%) depending on the varying capability of the velocity instruments to measure the uppermost portion of the section. The actual data coverage is shown in the figures by symbols (note that the gridding procedure has added about one grid point between each mooring).

For investigating the relationship between the currents and winds, we used data from the meteorological station at Point Barrow, Alaska, obtained from the National Climate Data Center of the National Oceanic and Atmospheric Administration. The weather station is located roughly 250 km to the west of the array site (Fig. 1). The meteorological data were first hand-edited to remove spikes (which occurred infrequently) and then linearly interpolated onto an hourly grid (S. Danielson, pers. comm., 2005). Data gaps greater than 6 h were not filled. The hourly 10-m wind observations were then low-pass filtered and subsampled to match the daily oceanic velocity data. No attempt was made to assess or remove sea-breeze/land-breeze effects in the wind timeseries. One would not expect a large diurnal sea-breeze signal at these latitudes (the sun is either generally up or down), and there should be very little signal in the winter months when ice cover is present.

To address how representative the winds at Pt. Barrow are compared to the mooring site, we accessed data from the ETA North American Mesoscale weather forecast model (ETA/NAM). The Atmospheric Research Measurement program has archived this high-resolution product from the National Centers for Atmospheric Research as part of the Alaska North Slope project. Grid #242 of the model covers our region of interest with a resolution of 12 km. We note that the ETA/NAM model is not a re-analysis product, and the Pt. Barrow wind data are not assimilated into the model. While it is beyond the scope of this study to do a comprehensive comparison over the year-long study period (the forecast model output is quite cumbersome to work with), we did a detailed comparison of a single storm in early November 2002. It was found that the ETA/NAM model accurately captured the winds at Pt. Barrow for this event both in amplitude and phase. According to the model, the winds at the mooring site were

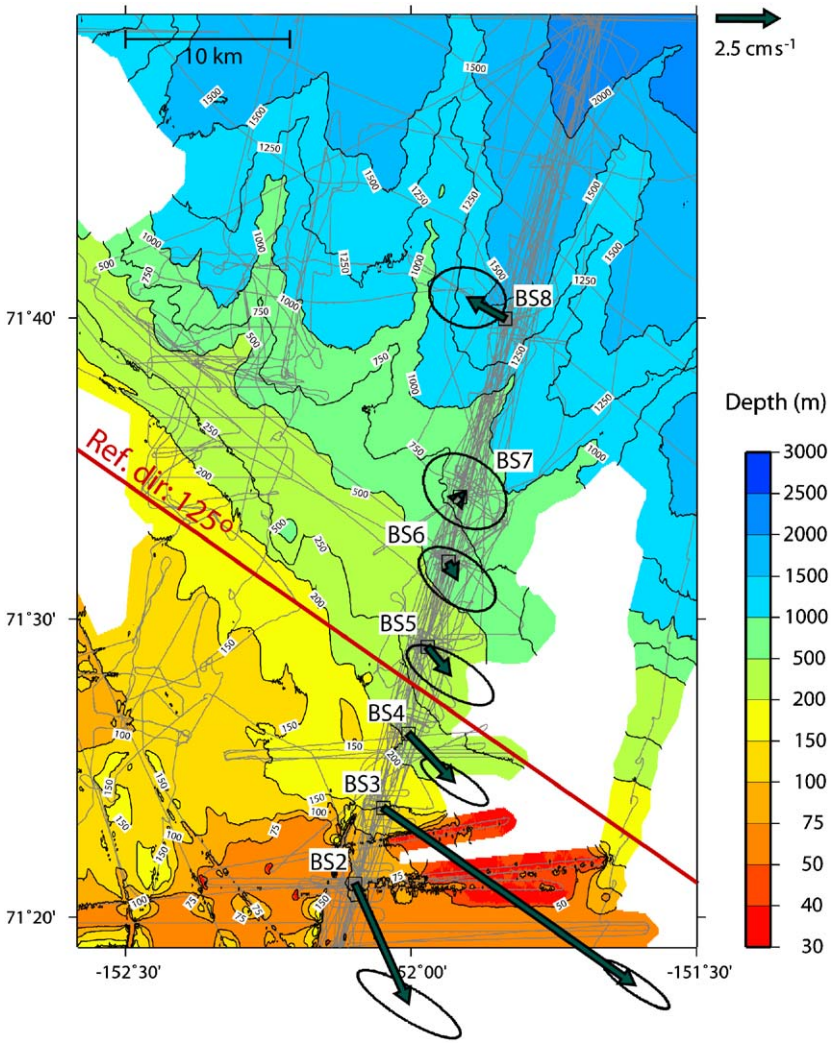

Fig. 3. Mean vectors and associated standard error ellipses superposed on the bottom topography (color) measured using shipborne multi-beam (gray lines denote the ship tracks). The means are for the year of August 2002–July 2003 (for BS8 only until March 2003) and averaged over 50–150 m depth. The red line shows the chosen alongstream direction of 125°T. Vectors and ellipses follow the scale in the upper right corner of the figure.

similar in character to those at Pt. Barrow. While the amplitude was smaller at the array site (65% of that recorded at Pt. Barrow), the timing of the wind peak was the same at the two locations within the 6-h resolution of the model output (correlation of $r = 0.92$). Based on this comparison, and in light of the large length scales of the storms that influence this region of the Beaufort Sea (Pickart et al., 2009b), we expect that the Pt. Barrow record is a reasonable proxy for the wind speed at the array site. This is further suggested by the high correlation between the westward flow reversals of the boundary current and the strong easterly wind events measured at Pt. Barrow (Tsimitri and Pickart, 2006; Spall et al., 2008).

3. Mean structure

We begin our presentation of the Beaufort shelf-slope velocity data by looking at the mean values for the year-long period of August 2, 2002–July 31, 2003. Fig. 3 shows the mean vectors at the individual mooring sites, averaged over the depth range 50–150 m, which encompasses the bulk of the Pacific water component of the mean boundary current (see below). There is a clear signature of an eastward-flowing jet between sites BS2 and BS4 (recall that the shoreward-most mooring site, BS1, returned no velocity data). At these three sites the mean is greater than the standard error. Farther offshore the flow is more variable and the mean vectors are not significantly different from zero at the outer sites (keep in mind that both BS7 and BS8 had shorter record lengths over this depth range, Fig. 2). For the construction of the error ellipses we used an integral time scale of 1–8 days (the smallest values in the region of strongest flow and at depth). This corresponds to at least 22 degrees of freedom, defined as the record length divided by twice the integral time scale.

To shed light on the orientation of the mean flow across the array, we included the bottom topography on Fig. 3 as measured from the multi-beam system on the USCGC *Healy*. Over the time period 2002–2004 there were six different *Healy* cruises that collected swath bathymetry in the vicinity of our array. These data were incorporated, along with other multi-beam data in the Arctic, by the Hawaii Mapping Research Group into a composite data set. For details of the data collection and compositing process the reader is referred to the Arctic Archive for Geophysical Research website (http://www.soest.hawaii.edu/hmrg/Aagruuk) and Johnson et al. (2006). We downloaded the Alaska margin data set, and used a Laplacian-Spline interpolator to fill in the smaller data gaps. The resulting bathymetry, shown in Fig. 3,

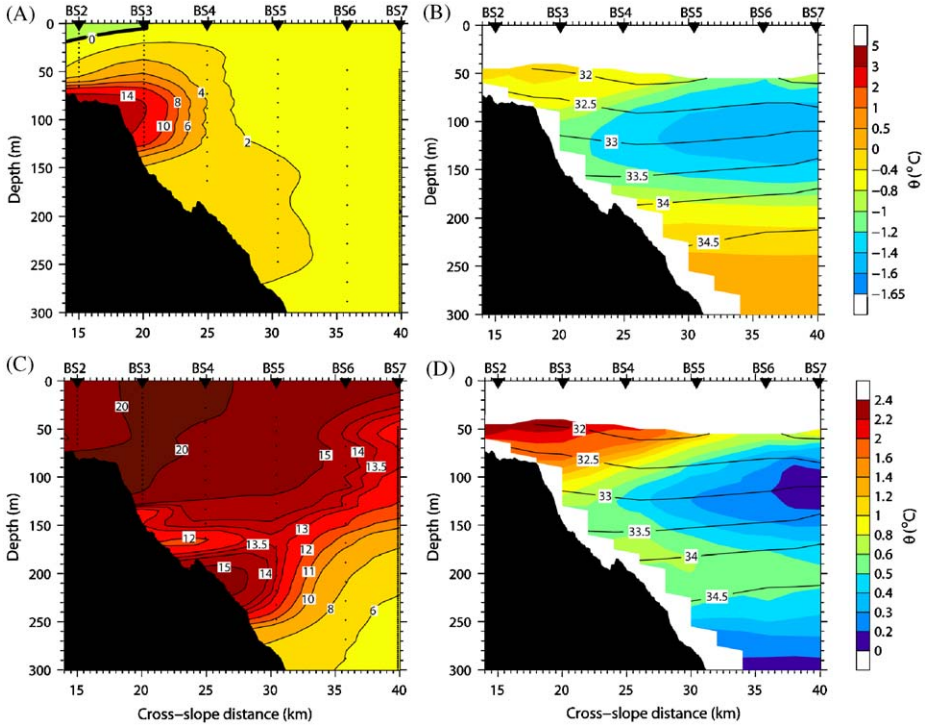

Fig. 4. Vertical sections of (A) mean alongstream velocity (cm s^{-1}) and (B) mean potential temperature (color) and salinity (contours), and (C, D) the associated standard-deviation fields of velocity and temperature for the year of August 2002–July 2003. Dots show the locations of the velocity measurements (note that (A) and (C) use different velocity color scales). The mooring sites are indicated at the top.

differs significantly from the International Bathymetric Chart of the Arctic Ocean (IBCAO) in this area, particularly on the outer shelf and over the deep slope. In general, the direction of the strongest mean flow is oriented along the upstream bathymetry (i.e. immediately to the west of the array line). A notable exception is the mean flow at the offshore-most site BS8, which is the only vector oriented to the west. However, since this record ended in March it is biased (relative to the other sites) by the fall/winter upwelling season, which is characterized by frequent westward flow reversals. The other notable feature is the increased southward component of mean flow at the shoreward-most site BS2. This is perhaps influenced by the southward excursion of the 75-m isobath associated with the ridge just upstream of the site.

Fig. 4 shows the mean vertical sections of gridded alongstream velocity and standard deviation. For comparison, the analogous mean potential temperature and salinity sections are included, along with the standard deviation in temperature. The reader is referred to Spall et al. (2008) for a description of the construction of the hydrographic vertical sections. This view reveals that, in the mean, the boundary current is a subsurface feature trapped to the shelf edge near 100 m depth (Fig. 4A). It is very narrow (width scale 10–15 km) with a core speed of approximately 15 cm s^{-1} and a deeper "tail" of 2–3 cm s^{-1} extending to 250 m depth. The mean temperature section (Fig. 4B) reveals that the boundary current advects three different water masses: summer Pacific water (shallower than 100 m on the inshore side of the section), winter-transformed water of Pacific origin (generally shallower than 150 m offshore of the shelfbreak), and Atlantic water (deeper than 150 m). The summer water consists of two separate water masses. The first is Chukchi/Bering summer water, which is resident over much of the Chukchi Sea in late summer, and also found in significant amounts in the Canada Basin (Shimada et al., 2001; Steele et al., 2004). Shimada et al. (2001) refer to this water mass as Western Chukchi Summer water, while Steele et al. (2004) call it Summer Bering Sea water. The second, and by far the most dominant summer water mass observed by the mooring array, is the warm and buoyant Alaskan Coastal water (Coachman et al., 1975), having been advected to this location by the Alaskan Coastal Current along the eastern boundary of the Chukchi Sea (Roach et al., 1995). Shimada et al. (2001) call this water mass Eastern Chukchi Summer water. Seasonally (late summer to early fall) the temperature of this water at our array site is much higher than the mean values seen in Fig. 4B. The winter-transformed water (colder than −1.2 °C) is coldest offshore of the core of the mean boundary current of Fig. 4A. This is because wintertime upwelling brings warm Atlantic water upslope, which moderates the mean temperature there. During the time period when the winter-transformed water is most prevalent (late spring to early summer), the coldest water is found adjacent to the continental slope (see below).

The Alaskan Coastal water, which seasonally occupies the inshore near-surface part of the section, is not directly associated with a distinct feature in the mean velocity section. However, a surface-intensified eastward-velocity signature appears in the composite mean of the summer months (see below). Evidence of this flow is also visible in terms of the large near-surface variability seen in both the velocity and temperature standard-deviation sections (Fig. 4C and D). The maximum values of velocity standard deviation (>20 cm s^{-1}) occur in a band extending from the shelfbreak at 100 m depth to near-surface levels. While the deeper part of this band indicates that the jet itself is at times much stronger than the average value of 15 cm s^{-1} (and that it sometimes reverses), the high variability at shallower depths reflects the seasonal surface-intensified eastward flow, associated with the considerably warmer and fresher Alaskan Coastal water in summer. Interestingly, both the velocity and temperature standard-deviation fields show an additional local maximum adjacent to the slope near 200 m depth, within

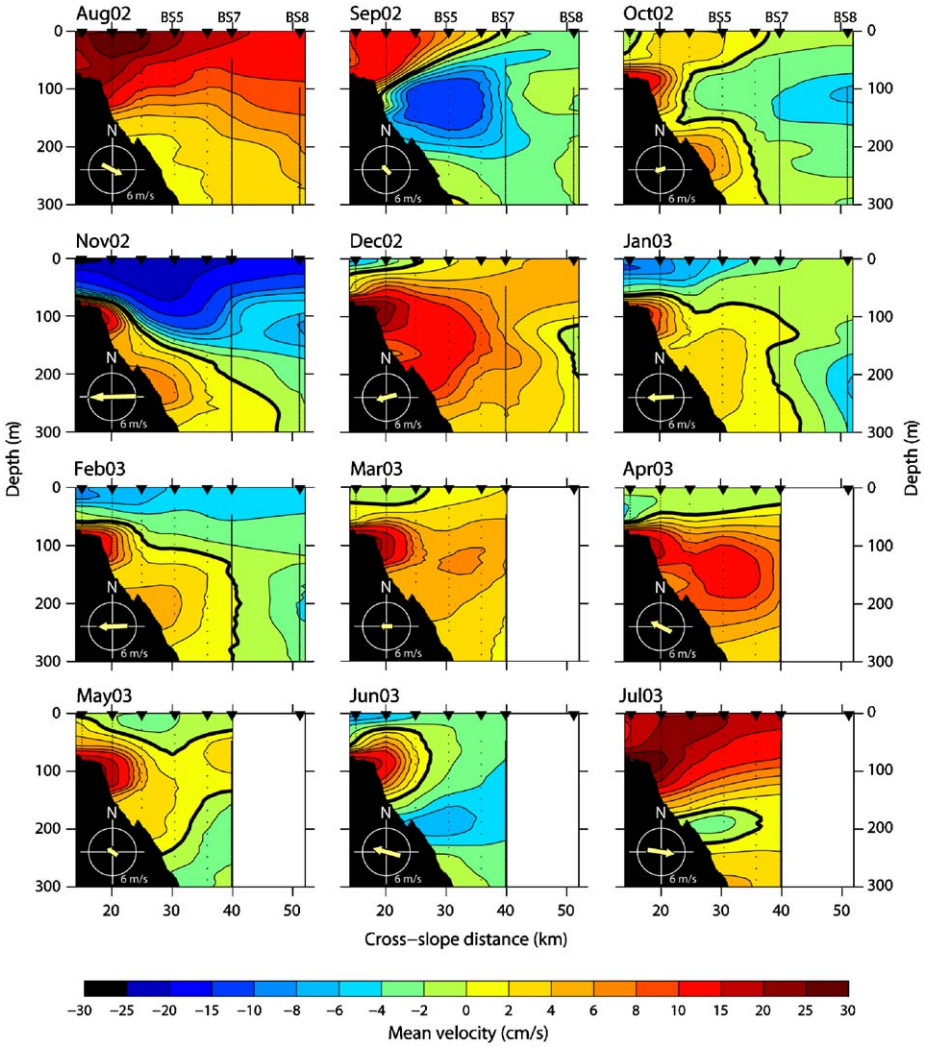

Fig. 5. Vertical sections of the monthly averaged alongstream velocity for August 2002–July 2003. Included are the monthly averaged 10-m wind vectors at Pt. Barrow (see also Fig. 6). The compass-circle indicates wind velocities of 6 m s^{-1}. Other notations are as in Fig. 4.

the region of the deep velocity tail seen in the mean. As seen in the next section, these features in the variability are associated with upwelling events that occur mainly during the winter season.

The high-resolution, statistically robust mean characteristics of the shelf-edge boundary current presented here have sharpened our view of the circulation on the Beaufort shelfbreak and slope. Earlier less detailed measurements suggested a somewhat different view. Aagaard (1984), based on four years of mooring data, reported a mean eastward motion along the shelf on the order of 10 cm s^{-1} between 146° and 152°W. Seaward of this he argued that the flow intensified down to the base of the continental slope (1000 m), a feature that he called the Beaufort Undercurrent. Later, Pickart (2004) compiled historical hydrographic data, collected between 140° and 153°W, to create a mean absolute geostrophic velocity section. This revealed a fairly narrow current, which was called the Beaufort shelfbreak jet, centered between 150 and 200 m depth and intensified along the upper continental slope. The data presented here indicate that in the mean the western Arctic boundary current is bathymetrically trapped to the shelfbreak, with only weak flow of 1–2 cm s^{-1} over the deeper slope, offering a new view of the velocity structure along the boundary of the Beaufort Sea.

4. Temporal variability

4.1. Seasonal trends

To examine the evolution of the boundary current over the course of the year, monthly composite vertical sections of the alongstream velocity were constructed (Fig. 5). To shed light on the possible causes of the monthly variation we also computed the monthly mean 10-m wind vectors at Pt. Barrow (shown separately in each monthly plot of Fig. 5, and all together in Fig. 6). It is clear that the flow at the array site can be considerably different than the mean (Fig. 4A) during certain times of the year. The eastward subsurface jet is present during most months, but the flow over the rest of the section, especially in the near-surface layer, is subject to large seasonal variability. Persistent easterly winds, occurring mainly during the fall/winter season, give rise to strong westward surface flow as can be seen for the months of November, January and February. The surface-intensified eastward flow in summer (July–September) occurs during periods of reduced easterly or even westerly winds and is associated with a strengthening of the Alaskan Coastal Current which brings warm, buoyant water past Barrow Canyon (Mountain et al., 1976; Münchow and Carmack, 1997; Pickart et al., 2005).

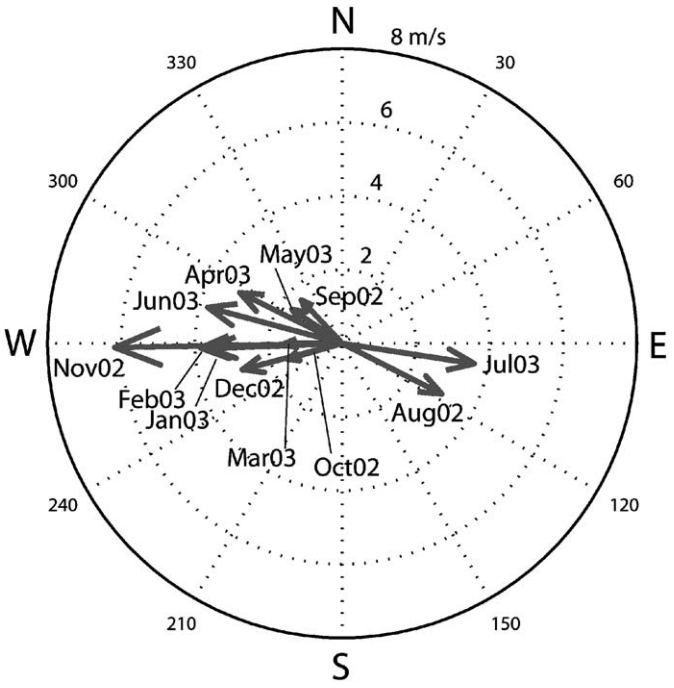

Fig. 6. Monthly averaged 10-m winds computed using the daily low-passed observations from Pt. Barrow weather station (see Fig. 1).

Overall, three dominant seasonal flow regimes emerge that are highlighted by the composite averages in Fig. 7. In spring the boundary current consists of a subsurface core trapped to the shelfbreak (Fig. 7A); this is much like the mean state of the current (without the deep tail), although the flow in the near-surface layer is weakly to the west. During this time of the year the current is primarily advecting winter-transformed Pacific water (Fig. 7B), with the coldest temperatures found in the upper halocline (salinity of 32.5–33.0). For more details on the structure of the boundary current during springtime, the reader is referred to Spall et al. (2008). In summer the eastward current is surface-intensified (Fig. 7C). Again it is strongest at the shelfbreak, but strong velocities extend well offshore. The hydrography indicates that warm, fresh Alaskan Coastal water occupies much of the boundary current during this time period (Fig. 7D). Finally, in winter, a subsurface core of eastward velocity is again centered at the shelfbreak, but in contrast to the springtime period (the first case above) there is a second eastward-velocity core at roughly 250 m, as well as strong westward flow above 50 m (Fig. 7E). This state of the current is reflective of upwelling conditions under enhanced easterly winds (Fig. 6), where warm Atlantic water is found upslope and the isohalines shoal toward the inshore part of the section (Fig. 7F). These three seasonal regimes of the boundary current are consistent with the findings of Pickart (2004), who analyzed a collection of historical hydrographic sections spanning many years (the seasonal timing is slightly different in the present data set, but one should keep in mind that we are considering only 1 year of data in this study).

While the seasonal characteristics of the boundary current from our direct velocity data are in line with Pickart (2004) (who used subjectively referenced thermal wind fields to describe the seasonality in velocity) a number of additional features are present in our monthly averages (Fig. 5). For example, in September 2002 there was a strong subsurface flow reversal (to the west) seaward of the jet core at the shelfbreak, resulting in a very strong velocity shear. Another subsurface reversal occurred in June–July 2003 but the westward flow was weaker, spatially smaller, and centered deeper in the water column (also behaving differently in the individual daily sections). Perhaps the most prominent feature, however, is the one already indicated by the velocity standard-deviation field in Fig. 4C: the enhanced eastward-velocity core centered near 200 m during the fall and winter months (see for instance October 2002). Sometimes this feature is manifested as a deep extension, or tail, of the current, while at other times it corresponds to an extremum of eastward velocity (i.e. separate from the eastward-flowing core near the shelfbreak). The signature of this feature appears in the winter seasonal configuration (Fig. 7E) as well as in the overall mean section (Fig. 4A). We discuss the nature of this component of the boundary current further below.

4.2. Modes of variability

To investigate the dominant variability of the boundary current during certain times of the year, we performed various empirical orthogonal function (EOF) analyses using the gridded along-stream-velocity sections. For a description of the methodology the reader is referred to Pickart et al. (1999). The first EOF calculation was done using all 364 daily realizations from August 2, 2002 to July 31, 2003. The first-mode vertical structure of the alongstream velocity and the modal amplitude timeseries are shown in Fig. 8. This mode explains 63% of the record variance, which is more than four times the 14% accounted for by the second mode (not shown). The presentation in Fig. 8 is such that the vertical structure represents the maximum dimensional value of the mode. Hence the mode is characterized by velocity variability as strong as $70\,\mathrm{cm\,s^{-1}}$ in the vicinity of the shelfbreak.

To illustrate what this means for the alongstream-velocity structure, we added ± 1 standard deviation of the modal amplitude back into the mean field (Fig. 9). In the positive modal extreme (Fig. 9A), there is enhanced eastward flow of the shelfbreak-trapped current. The current is both vertically and horizontally more widespread than the mean, with a considerably stronger core velocity. The negative modal extreme is characterized by westward velocities over the entire section (Fig. 9B), with peak velocities occurring at near-surface levels over the upper slope. The interpretation of this mode is that it captures the eastward-flowing state of the current under weak or westerly winds versus the easterly wind-forced reversed state. The former case is a combination of the summertime flow of the Alaskan Coastal Current extension (which is why significant eastward flow extends to the surface) and the bottom-intensified jet during the rest of the year. The associated timeseries for this mode shows a hint of seasonality (more positive values during winter than summer, Fig. 8B), and is weakly (but significantly, $r = 0.57$) correlated with the wind speed record from Pt. Barrow. It also contains a signature of significant storm events throughout the year.

In order to clarify further the response of the boundary current to upwelling storm events, we carried out a second EOF calculation by isolating that part of the record associated with strong easterly winds. Tsimitri and Pickart (2006) developed an objective approach for identifying upwelling events over the year-long record. Essentially, an event occurred when three criteria were satisfied: strong easterly winds, reversed (westward) flow, and the appearance of warm, salty water at shallow depths (i.e. upwelled Atlantic water). We isolated these events and constructed a timeseries of upwelling (including the events themselves plus the time periods immediately before and after) consisting of 72 out of the total 364 days. Since the BS8 velocity record (which ended in late-March) captured nearly all of these realizations, it was included in the calculation (using 68 realizations), resulting in a larger domain EOF (14–52 km, 0–1000 m).

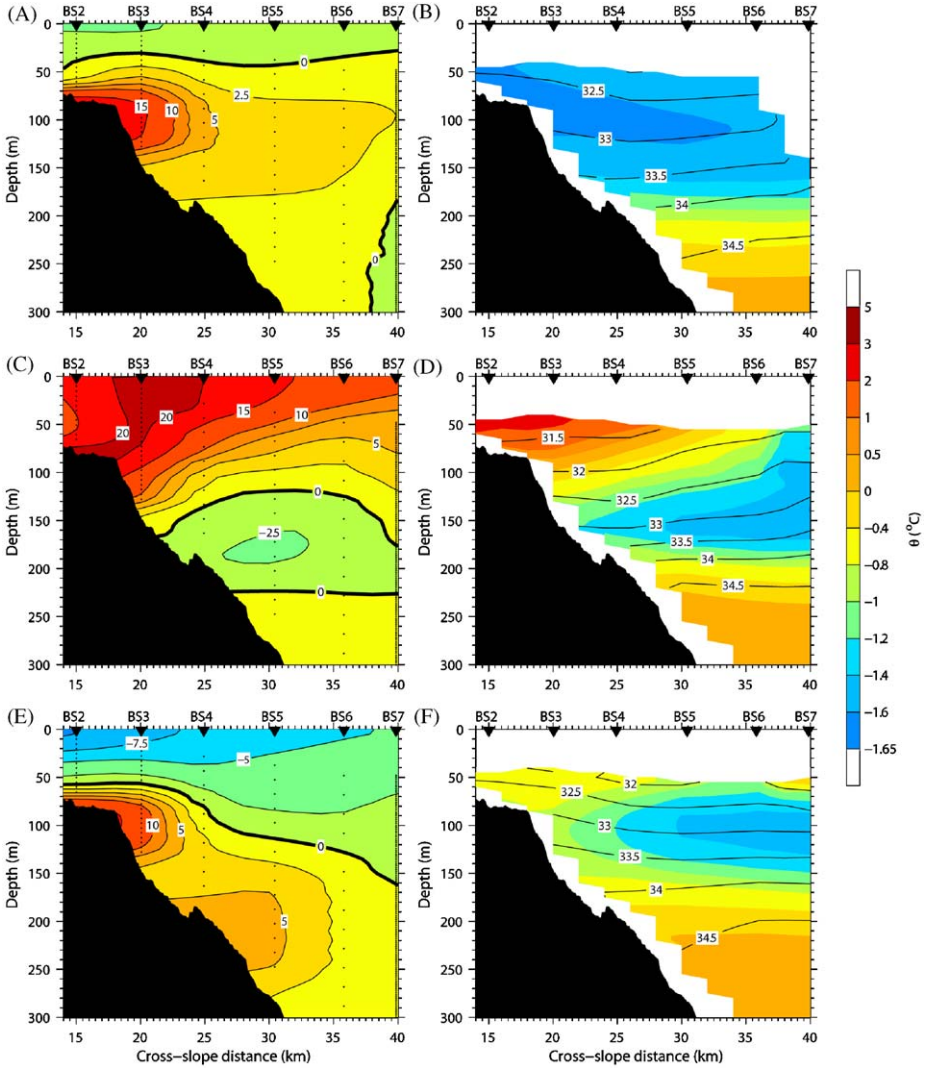

Fig. 7. Vertical sections of the composite averages of velocity, potential temperature and salinity for (A, B) spring: March–June 2003; (C, D) summer: August–September 2002 and July 2003; (E, F) winter: October 2002–February 2003. Notations as in Fig. 4. Note that the velocity color scale is different from Figs. 4 and 5.

Fig. 10 shows the distribution of these realizations over the course of the year.

The first EOF mode for this subset of the record explains 69% of the variance (Fig. 10). The addition of ± 1 standard deviation back into the mean shows a strong surface-intensified westward flow during the height of the storms (Fig. 10A, negative extreme), and an eastward-flowing shelfbreak jet with a strong deep extension during the periods bracketing the storms (Fig. 10B, positive extreme). Note that the signature of this mode extends quite deep and far offshore. The eastward velocities in the deep tail are of the same order as those of the mean shelfbreak jet itself. Inspection of the individual daily sections reveals that the deep eastward-flowing core forms shortly after the storm abates. Performing an EOF calculation on the remaining 292 "non-upwelling" realizations, it is found that this feature is absent from the dominant mode (which explains 59% of the variance, not shown). This explicitly demonstrates that the deep tail of the boundary current in the winter composite (and in the year-long mean section) is associated with the occurrence of upwelling storm events in the southern Canada Basin. It also indicates that the direct influence of the wind extends to depths of 800–1000 m.

It is not obvious what causes the flux of eastward momentum to deeper depths following the storms, but, as a result, the underlying Atlantic water is accelerated during the fall and wintertime period. Synoptically (i.e. shortly after a storm) this flow can exceed 40 cm s^{-1} with strong lateral velocity shears. This in turn might lead to conditions favorable for barotropic instability and eddy formation. Observations in the southern Canada Basin have revealed both cyclonic and anti-cyclonic eddies of Atlantic water (D'Asaro, 1988; S. Zimmermann, pers. comm., 2007) whose origin may be related to this. A synoptic shipboard velocity section occupied 300 km to the west across the Chukchi shelfbreak, during upwelling conditions, showed a similar double-core boundary current structure (Llinas et al., 2008). This suggests that the double-core signature of the boundary current is not confined to the geographical area near the array. Further work is necessary to understand the dynamics of this energized state of the deep component of the western Arctic boundary current.

5. Transport

The long-term average transport of Pacific water flowing northward through Bering Strait is approximately 0.8 Sv (Roach et al., 1995; Woodgate et al., 2005a). Within the Chukchi Sea the majority of the flow is believed to follow three different branches

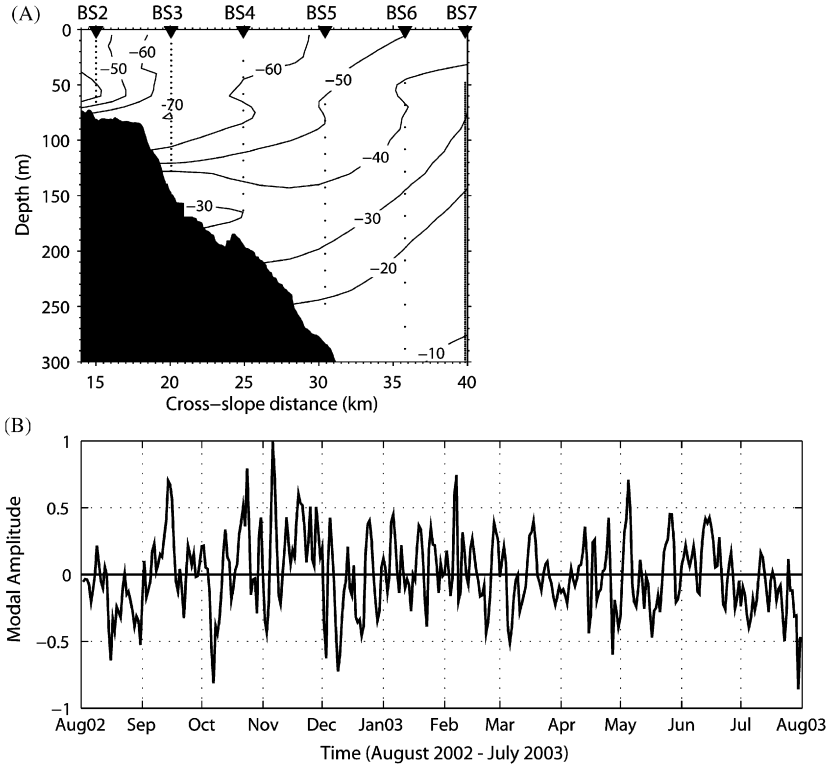

Fig. 8. Dominant EOF mode for all 364 daily realizations in the alongstream-velocity record, explaining 63% of the variance: (A) Vertical structure and (B) modal amplitude timeseries.

(Fig. 1): one to the west through Hope Valley into Herald Canyon; one to the east along the coast of Alaska into Barrow Canyon; and the third branch flowing through the Central Channel between Herald and Hanna Shoals (Weingartner et al., 1998; Woodgate et al., 2005b). While the flow through the Central Channel is not very well described, observations suggest that the outflow emerging from Herald and Barrow canyons (accounting for 75% of the total Bering Strait transport; T. Weingartner, pers. comm., 2005) occurs mainly on the eastern sides of the canyons (Münchow and Carmack, 1997; Pickart et al., 2005; Whitledge, 2006). Based on geostrophic dynamics then (in the absence of wind), the Pacific water should be largely constrained to follow the isobaths and turn eastward to form a boundary current along the edge of the Chukchi and Beaufort shelves (rather than, say, flowing directly across the continental slope into the deep basin). Recent model results suggest that this is the case (Winsor and Chapman, 2004; Spall, 2007), and evidence from radium isotope analysis supports this notion as well (Kadko and Muench, 2005). If this topographic steering is complete, then we would expect to find roughly the same amount of Pacific water passing by our Beaufort array site as that which flows through Bering Strait.

5.1. Determining the Pacific/Atlantic water mass boundary

In order to separate the measured volume transport at our array into Pacific and Atlantic water components, it is necessary to define the boundary between the two water masses. This was done using the potential vorticity computed from the mooring hydrographic data. In particular, the stretching component of the potential vorticity $PV = -(f/\rho)(d\rho/dz)$ was used, where f is the Coriolis parameter and ρ the density. We note that this is akin to using the stratification (buoyancy frequency). The deepest and densest part of the Pacific water is the winter-transformed water, which is characterized by weak stratification, or low PV, because it is formed on the Bering and Chukchi shelves through convective overturning (e.g., Weingartner et al., 1998). Although the formation occurs during the winter months only, the signature of this water mass is present throughout the year at the array site. This is likely due to a number of reasons. First, the draining of the dense water from the Chukchi shelf takes place over a number of months. For example, winter-transformed water has been observed flowing northward through Barrow and Herald Canyons in late summer (Münchow and Carmack, 1997; Pickart et al., 2005; Whitledge, 2006). Second, the distance from Herald Canyon to 152°W is more than 800 km, so some of the winter water has a long way to travel before reaching the array. Third, the frequent flow reversals of the boundary current, due to easterly winds, will delay the signal even further. Regardless of the precise reasons, some amount of winter-transformed water was detected in every realization during the first deployment of the array (note the presence of the cold winter water in all three seasonal composites of Fig. 7).

One of the consequences of the weakly stratified winter water, which can be thought of as a mode water, is that it compresses the density surfaces both above and below the layer. This has ramifications for the stability of the boundary current and its ability to form eddies (see Spall et al., 2008). It also means that the water mass boundary between the winter water and the underlying Atlantic water is characterized by a well-defined layer of high PV. We used the center of this layer as the boundary between the Pacific and Atlantic water. In particular, the hydrographic mooring data were used to construct daily vertical sections of PV, and the cross-stream distribution of the high PV layer was in turn tabulated (see Fig. 11). This procedure was carried out manually for each of the 364 realizations, but we stress that it was an objective process.

As a check on this approach, we considered the nutrient data collected at the array site over the course of the SBI program.

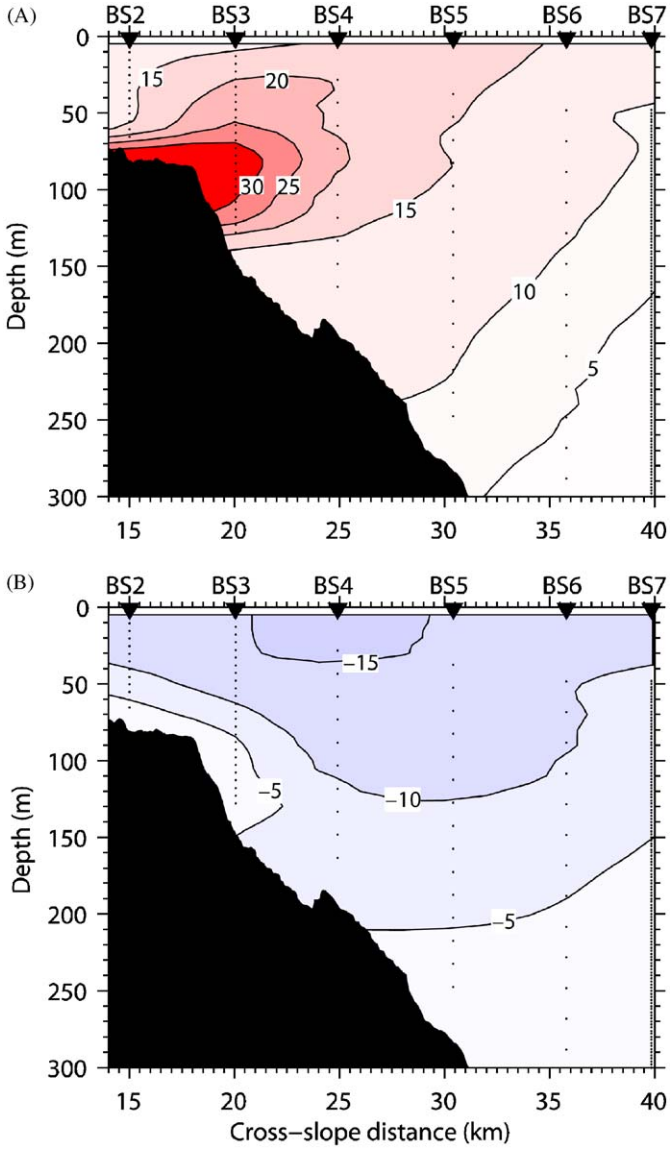

Fig. 9. One standard deviation of the modal amplitude in Fig. 8 (A) added to and (B) subtracted from the mean velocity field (shown in Fig. 4A).

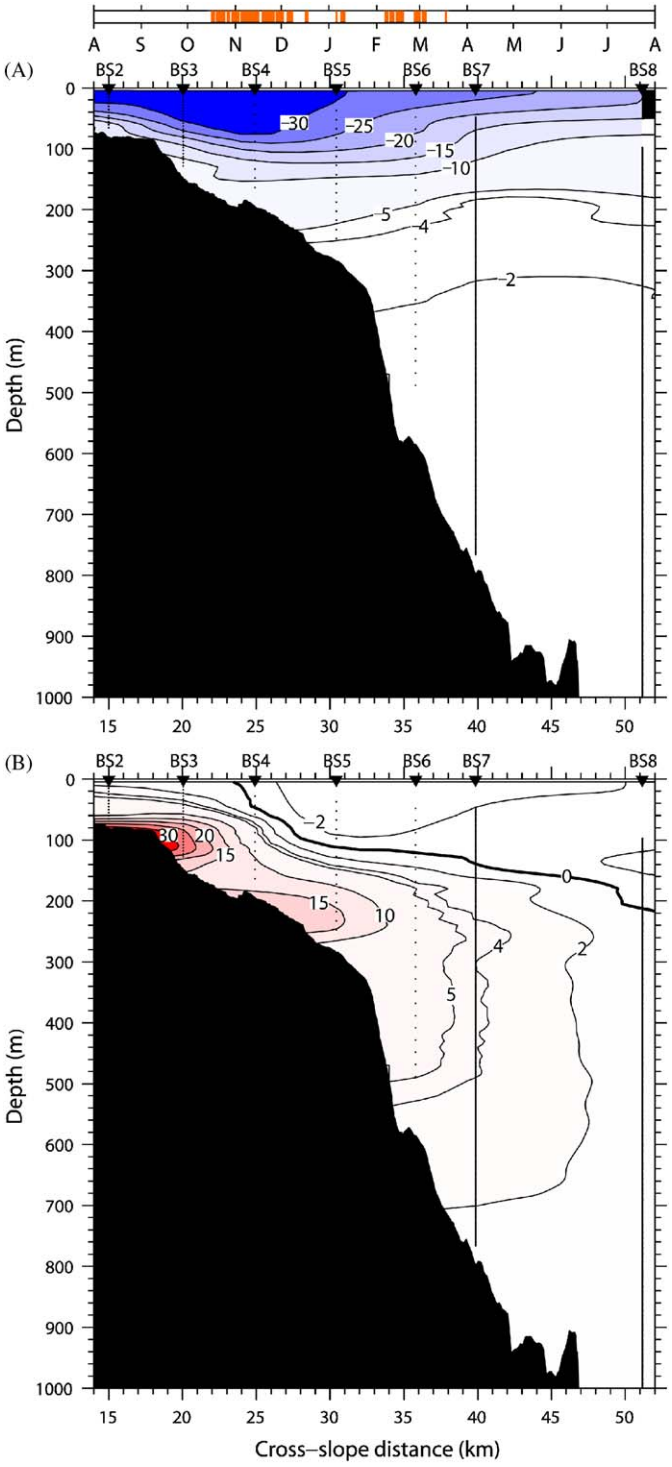

Fig. 10. Dominant EOF mode for 68 daily realizations of the alongstream-velocity record during upwelling periods. The dates of the realizations, during the period August 2002–July 2003, are indicated in the time bar at the top. Shown is one standard deviation of the modal amplitude (A) subtracted from and (B) added to the mean velocity field (cf. Fig. 9).

During the two-year period there were a number of shipboard hydrographic crossings near 152°W, and, following the methodology of Jones et al. (2003), we used the nitrate/phosphate relationship to compute vertical sections of Pacific-water fraction. The boundary between the Pacific and Atlantic waters is characterized by a large gradient in this fraction, and we used a value of 0.6 as the delimiter (keep in mind there is some uncertainty in the location of the boundary computed as such because of the bottle spacing across the sections). Next we applied the PV gradient technique to the corresponding shipboard CTD density sections. (Here we were able to increase the lateral resolution by using the expendable CTD casts taken between the bottle stations.) The comparison between the two approaches is shown in Fig. 12. The high PV layer at the base of the winter water is clearly evident, and the solid line marks the center of the layer. The dashed line is the water mass boundary computed from the nutrient relationships. One sees that, overall, the results from the two independent methods are consistent with each other, which provides additional confidence in the PV approach. Note that in four of the shipboard realizations the nutrient data indicate that Pacific water is not present in some parts of the surface layer. It is impossible to say anything about this shallow upper boundary using the PV data (plus the mooring hydrographic measurements extended only to 50 m). This source of error for the Pacific water transport is discussed below.

It is of interest to consider the characteristics of the Pacific/Atlantic water mass boundary as computed from our year-long

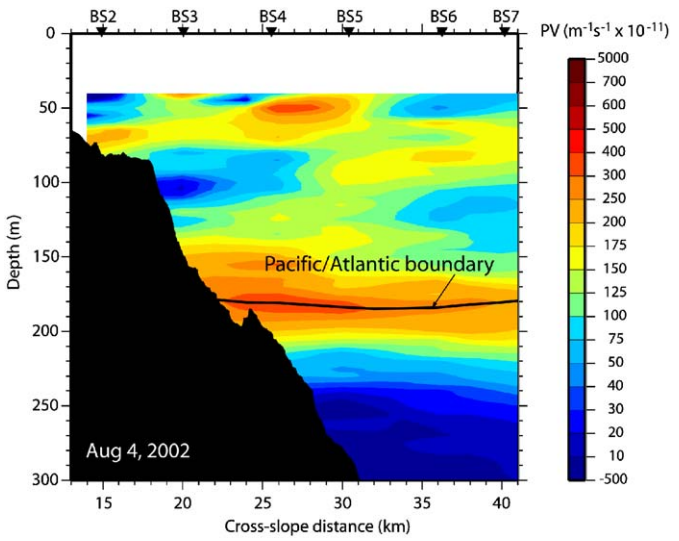

Fig. 11. Snapshot of stretching potential vorticity (PV) from the mooring array, showing the high PV layer at the base of the winter-transformed Pacific water. The black line denotes the center of the layer, which is used as the boundary between the Pacific and Atlantic water masses for the transport calculations.

timeseries of hydrographic sections. For each daily realization we computed the average properties of the boundary across the section. Fig. 13 shows the variation in depth of the boundary over the course of the year. The year-long average value is 140 m. It is deepest in spring and early summer when the volume of winter water is greatest (see Spall et al., 2008), and it is shallowest (less than 100 m) during upwelling events in the late-fall and winter months. Overall the depth variation is not very pronounced, with a standard deviation of only 25 m. By contrast, the hydrographic properties of the boundary vary significantly throughout the year. Fig. 14 shows the scatter plot of the boundary T/S, where the year has been divided into roughly the same three seasonal regimes as in Fig. 7. (Here we have included the month of October in the summer regime.) For comparison purposes, we display these daily boundary values in relation to the T/S distribution of the time-mean section (gray symbols). The majority of the daily values fall along the mean envelope; however, there are significant excursions. Most notably, the water mass boundary is anomalously warm and fresh during part of the summer season (red circles), while it is anomalously cold and salty during a portion of the spring season (blue circles). Averaged over the entire year, the Pacific/Atlantic water mass boundary lies at a temperature of $-1.26\,^{\circ}C$, salinity of 33.64, and density of $27.06\,kg\,m^{-3}$ (denoted by the black/yellow square in Fig. 14).

5.2. Mean transport

Using the water-mass boundary as defined above, we computed the transport of both the Pacific and Atlantic components of the boundary current. This was done using the gridded velocity sections presented above, where the bottom triangles over the continental slope were filled by simple extrapolation. Due to the shorter record length of the outermost/deepest mooring (BS8), the domain for the full-year transport calculation was confined laterally between BS2 and BS7 and vertically between 0 and 800 m. However, for reference, the transport was also calculated for a larger domain (BS2–BS8, 0–1400 m) for the time period of August 2002–March 2003 (see below and Table 1).

The sources of error for the mean transport are as follows. The instrument uncertainties (discussed earlier) are ± 0.5 and $\pm 2\,cm\,s^{-1}$ for the ADCPs and ACMs, respectively. It is assumed that these are uncorrelated across the array, which results in a transport error of 0.002 Sv for the Pacific water and 0.0025 Sv for the Atlantic water, respectively. To estimate the measurement uncertainties we constructed the co-variance matrix, whose diagonal elements were normalized by the degrees of freedom using the respective integral timescales (see Section 3). If all of the measurements were independent across the array, the transport error would be associated only with the diagonal elements. However, the close spacing of the moorings and the scales of variability were such that the cross-variances (off-diagonal terms) were non-negligible. Normalizing these by the mean number of degrees of freedom, the full measurement transport uncertainty is 0.074 Sv for the Pacific water and 0.022 Sv for the Atlantic water, respectively. There is also error associated with the gridding process. This was estimated by computing the residuals between the mean velocities at the measurement sites and the gridded values closest to those sites. Applying this over the entire section gives a transport error of 0.006 and 0.002 Sv for the Pacific and Atlantic components, respectively. Finally, over parts of the year there was likely river water present in the surface layer (e.g. from the Mackenzie River) as well as sea-ice melt water. Since the moored profilers extended only to 50 m, it is impossible to determine this from the array data. As mentioned above, the nutrient data from the shipboard crossings showed that some of the sections contained non-Pacific-origin water near the surface (Fig. 12). Assuming a layer 10 m thick for half the year, at the mean speed of the layer, gives a value of 0.002 Sv, which was subtracted from the Pacific-water mean value.

5.2.1. Pacific water

Considering all of these sources of error, the mean eastward volume transport of the Pacific water component of the boundary current is 0.13 ± 0.08 Sv for the year-long record. Note that this mean value is less than 20% of the long-term mean transport through Bering Strait. In light of the dynamical constraints mentioned above, as well as the recent modeling studies, this is a surprising result. It should be kept in mind, however, that our mean transport value is likely an underestimate. For example, note that the mean summertime configuration of the jet (Fig. 7B) extends seaward beyond our array. This is perhaps not surprising since the surface-intensified state of the jet during this time period will be less constrained by the bottom topography due to the large stratification (although to first order the jet does appear to be locked to the shelfbreak, Fig. 7B). There is also likely eastward flow inshore of BS2 on the shelf. Using the mean BS1 record from the second deployment as a guide for the shoreward part of the array, we estimate the missing eastward transport to be approximately 0.003 Sv. For the seaward side of the array, the truncated BS8 extends only to 100 m (less than 50% of the time, Fig. 2), so it cannot be used as a guide for the bulk of the eastward-flowing jet. Simple lateral extrapolation suggests that the offshore contribution is on the order of 0.01 Sv. Even accounting for these two contributions in transport, and considering the uncertainty described above, our results imply that, at most, only about 30% (0.22 Sv) of the Bering Strait inflow ends up in the boundary current north of Alaska. Possible reasons for this are discussed in Section 6.

5.2.2. Atlantic water

The mean transport of Atlantic water during the full-year period (domain BS2–BS7, 0–800 m) is 0.047 ± 0.026 Sv, with errors as discussed above. About 0.02 Sv (43%) of this eastward transport is shallower than 300 m (cf. Table 1), where the largest velocities are generally observed. However, as seen earlier (Fig. 10), during

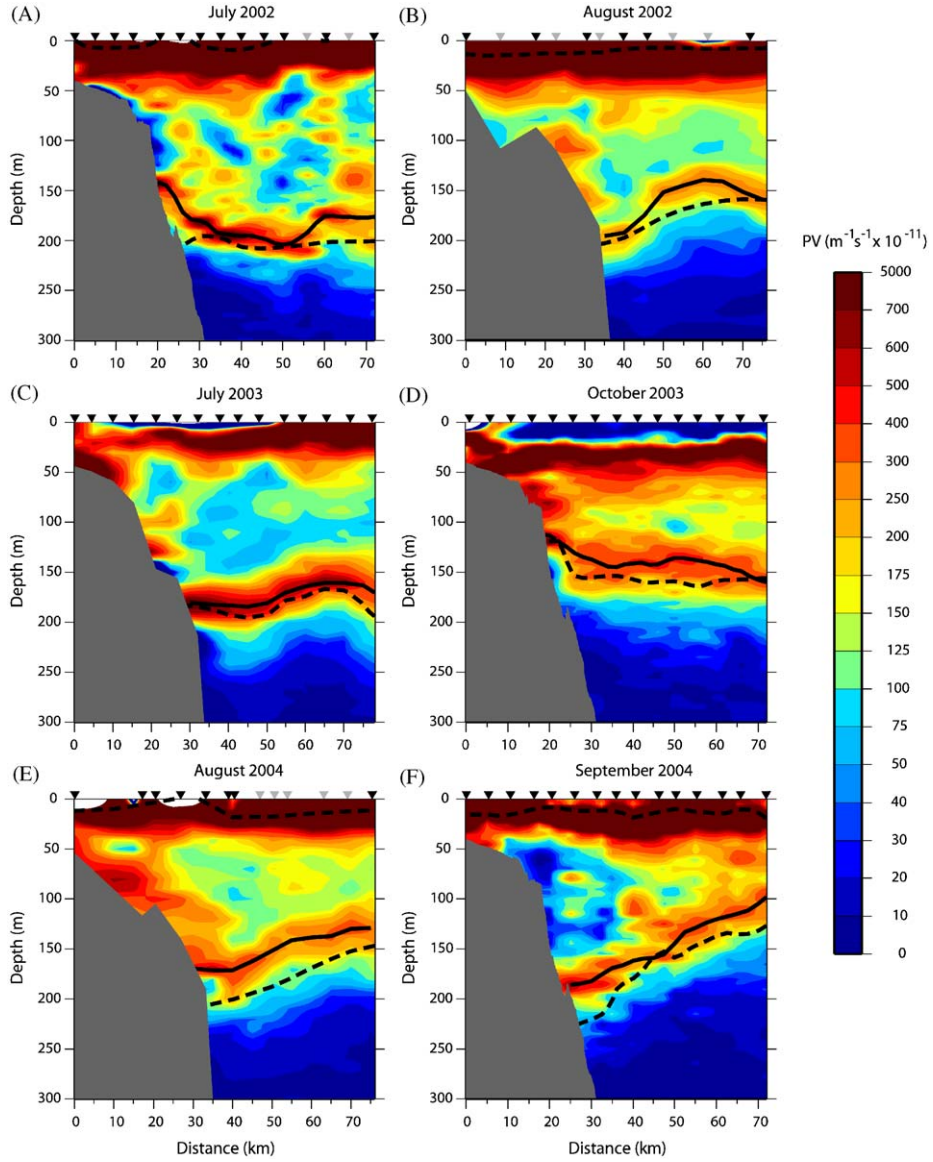

Fig. 12. Shipboard sections of stretching PV at the array site. The solid black line is defined as in Fig. 11, and the dashed black line denotes the Pacific/Atlantic water mass boundary defined using the nitrate/phosphate relationship (see text). The locations of the CTD/bottle stations are indicated by the black inverted triangles, and the expendable CTD casts are denoted by the gray inverted triangles.

upwelling events the wind-forced flow reaches deeper than this, with velocities of 2 cm s^{-1} down to 700 m depth. We have made no attempt to distinguish between the two varieties of Atlantic water, i.e. the Fram Strait branch water and Barents Sea branch water. As discussed by Schauer et al. (1997), these components become less distinct downstream of their confluence region in the Nansen Basin, due to mixing. Nonetheless, the Barents Sea branch water extends deeper in the water column (Schauer et al., 1997), and was observed to have elevated concentrations of CFCs in the density range 27.94–28.02 kg m^{-3} in the eastern Eurasian Basin (Smethie et al., 2000). (This corresponds roughly to a depth range of 500–1000 m near our array site.) Furthermore, the Fram Strait branch water is displaced offshore by the Barents Sea branch water as the latter exits the St. Anna Trough (Schauer et al., 1997, 2002a). These results suggest that there may be a significant amount of Atlantic water transport seaward of BS7 and deeper than 800 m. Accordingly, we computed the full-domain 8-month mean transport (August–March, BS2–8, 0–1400 m), but this only increased the Atlantic water contribution to 0.068 Sv (Table 1). One should keep in mind, however, that this time period is biased by the fall/winter upwelling season compared to the full-year record.

There have been very few estimates of Atlantic water transport in the Arctic Ocean with which to compare our value at 152°W. Atlantic water enters the Arctic through Fram Strait and the Barents Sea. Based on two years of mooring records in Fram Strait, Schauer et al. (2004) computed the Atlantic water transport on the eastern side of the strait to be 3.6 Sv (the sum of the Svalbard branch and the Yermak Plateau branch, although, according to the authors, some of this water may recirculate within the northern part of the strait). This transport is augmented downstream by the Barents Sea outflow through St. Anna Trough, which is estimated to be 1.9 Sv (Loeng et al., 1993; Schauer et al., 2002b). The combination of these two flows (5.5 Sv) is consistent with Woodgate et al.'s (2001) Atlantic water transport estimate of 5 Sv upstream (west) of the Lomonosov Ridge. It is believed that some portion of this water (primarily Barents Sea branch water, Rudels et al., 2004) stays on the continental slope past the ridge

into the Canadian Basin, while some of the water that is diverted northward makes it into the Canadian Basin via gaps in the ridge (Woodgate et al., 2001; Kikuchi et al., 2005).

Woodgate et al. (2001) calculate an Atlantic water transport of 3 Sv downstream (east) of the Lomonosov Ridge. It is worth noting that this value was obtained using velocity data from a single mooring only, which means there is inherent uncertainty. Also, Newton and Coachman (1974) computed an eastward transport of Atlantic water much smaller than this (0.3 Sv) along the continental slope of the Chukchi Sea. However, their value was derived from the dynamic topography of the 500 db surface relative to 1000 db, so it is undoubtedly an underestimate. Models give widely varying results regarding the circulation of Atlantic water in the Arctic Ocean (see Proshutinsky et al., 2005), although some studies show significant flow of Atlantic water east of the Lomonosov ridge circulating cyclonically around the Canadian Basin (Karcher and Oberhuber, 2002). Using a regional version of the Los Almos National Laboratory Parallel Ocean Program with 1/12° resolution (Maslowski et al., 2004), the mean transport of Atlantic water during 2002–2004 (the time period of SBI) along the Chukchi slope is calculated to be 0.73 Sv (W. Maslowski, pers. comm., 2007). Based on all of the above, it is evident that a significant discrepancy exists between our small Atlantic water

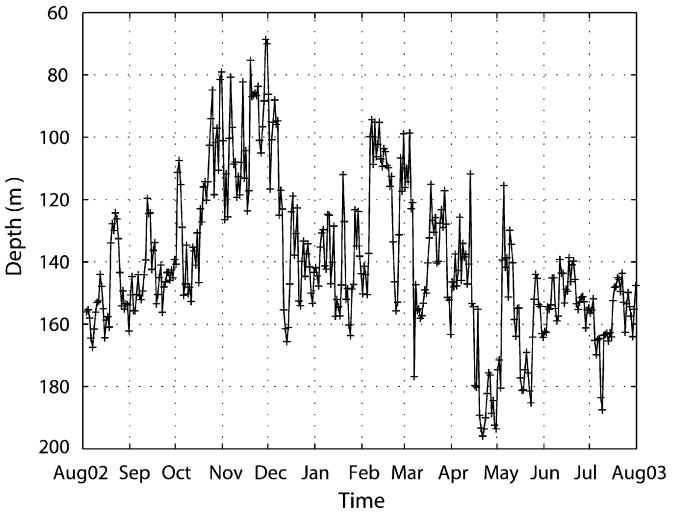

Fig. 13. Timeseries of the mean depth of the Pacific/Atlantic boundary, as computed from the hydrographic sections. The year-long average is 140 m.

Table 1
Mean transport values for the given time periods and spatial domains.

Time period	Domain	Total transport (Sv)	Pacific water (Sv)	Atlantic water (Sv)
August 3, 2002–July 31, 2003	BS2–BS7 (x = 14–40 km) d = 0–300 m	0.150	0.129	0.021
	BS2–BS7 (x = 14–40 km) d = 0–800 m	0.176	0.129	0.047
August 3, 2002–March 21, 2003	BS2–BS7 (x = 14–40 km) 0–300 m	0.100	0.070	0.030
	BS2–BS7 (x = 14–40 km) 0–800 m	0.135	0.070	0.065
	BS2–BS8 (x = 14–52 km) 0–1400 m	0.143	0.075	0.068

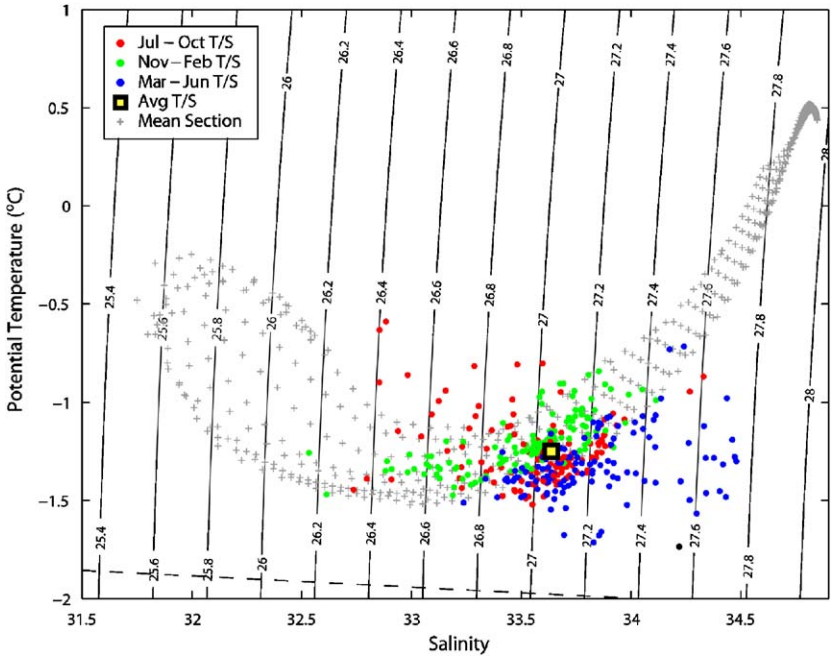

Fig. 14. Scatter plot of potential temperature and salinity overlaid on contours of density. Gray crosses show all T/S points from the year-long mean section (Fig. 4B). They extend from the warm/fresh Alaskan coastal water near the surface, through the Pacific winter water, to the warm, salty Atlantic water at depth. The red, green and blue symbols show daily T/S values of the Pacific/Atlantic boundary (the cross-stream average of the water mass boundary on that day) during roughly the same seasonal regimes as in Fig. 7. The black/yellow square denotes the year-long average boundary T/S.

transport value along the Beaufort slope and what is believed to flow through the Canadian Basin.

There are several factors that may help account for this disparity in transport. First, some of the Atlantic water entering the Makarov Basin is believed to recirculate along the Mendeleyev ridge before entering the Canada Basin (Rudels et al., 1994). Second, the Fram Strait branch of the Atlantic water seems to be less constrained to the continental slope (Schauer et al., 1997, 2002a) and can even shift laterally with season (Dmitrenko et al., 2006). This suggests that the SBI array may not have extended far enough offshore to bracket the flow (even with BS8). Third, the flow of Atlantic water in the Canadian Basin seems to be impacted by the regional wind field associated with the Arctic Oscillation (AO). For example, in the model of Karcher et al. (2007), during periods of enhanced anti-cyclonic wind forcing over the Canadian Basin, the (cyclonic) flow of Atlantic water around the periphery of the basin is diminished. According to Proshutinsky and Johnson's (1997) Arctic Ocean Oscillation index, the Canadian Basin has been in an anti-cyclonic regime since 1997 (during which time the AO has been generally low). Finally, there may be some diversion of Atlantic water from the boundary current into the interior of the Canada Basin in the vicinity of the Northwind ridge (i.e. upstream of our array site). Using temperature data, Shimada et al. (2004) revealed a tongue of Atlantic water extending offshore from the northern part of the ridge, which is consistent with elevated values of CFCs measured in this same area of the interior basin (Smethie et al., 2000). At this point, it is unknown which of these factors (or others) may be responsible for our small mean value of Atlantic water transport at 152°W.

5.3. Time variation

The timeseries of the daily net volume transport in the alongstream direction over the course of the year is shown in Fig. 15. Each daily data point was obtained by summing up the portion of Pacific and Atlantic water, respectively, in the gridded vertical section for a set of different domains, as described above and shown in Table 1.

The variability in transport is large, with values frequently exceeding 0.5 Sv in both the eastward and westward direction, for both the Pacific water and Atlantic water. Inspection of the individual sections reveals that the days of westward peak transport (<-1 Sv) are typically associated with high negative velocities extending laterally over much of the array, corresponding to upwelling storm events. However, the days of eastward peak transport (>1 Sv) mirror varying flow conditions depending on season. In late summer/early fall these peaks typically coincide with intensified surface-flow associated with the extension of the Alaskan Coastal current, i.e. predominantly Pacific water. The eastward peaks during the winter months are associated with the enhanced eastward velocity following the upwelling events (both the upper and lower velocity cores, e.g. Fig. 10A). In this case the major contributor to the transport is the Atlantic water. During spring and early summer (May and onward) the maximum eastward transport occurs for a variety of flow situations.

There is some degree of seasonality in the Pacific water transport series. The months between October and January are, with some exceptions, associated with significant westward net transport through the array, while the summer months of July and August are characterized by predominantly eastward transport. This tendency is emphasized by the 30-day running mean, superposed on the daily values in Fig. 15A. During the rest of the year, and on shorter timescales, the flow alternates between the two directions in a fairly regular manner. The Pacific water contribution from the offshore-most region (i.e. the laterally extended domain to BS8) is not especially large (Fig. 15A), as expected due to the smaller velocities there.

Because the boundary current, in general, is trapped to the shelfbreak, and since the bulk of the transport is contained in the upper 150 m of the section (not shown), this suggests that the velocity record from BS3 alone (the shelfbreak mooring at 147 m depth) could be used as a reasonable proxy for the complete Pacific water transport. This indeed seems to be the case. Comparing the timeseries of the vertically integrated alongstream velocity at BS3 to the Pacific water transport timeseries, we find that the agreement is excellent (Fig. 15A), with a correlation of $r=0.87$. Thus, due to the small lateral scale of the current and the strong role of the shelfbreak bathymetry, we can capture the dominant transport signal of the Pacific component of the boundary current using a single mooring. This implies that future monitoring of the current could be carried out with minimal instrumentation.

The seasonality of the Atlantic water transport is more prominent than for the Pacific water. In particular, note the increased variance during the months of October–January (Fig. 15B). This time period is, as discussed above, characterized by repeated upwelling events associated with strong westward flow during the storms and enhanced eastward flow in the period between the storms. During these events most of the transport is confined to the upper 300 m (Fig. 15B). Unlike the Pacific water, the lateral extension of the (800 m) Atlantic water transport domain to BS8 results in large contributions for both the eastward as well as westward flow. One reason for this is the large area that is added (about 8.8×10^6 m^2) to the transport section. However, as seen in Fig. 10, significant velocities can be found well offshore of the shelfbreak. The extension of the domain down to 1400 m results in just a small difference in transport (Fig. 15B).

5.4. Relationship to wind

As discussed above, the flow along the shelfbreak and upper slope of the Beaufort Sea is, to a large degree, forced by wind. During upwelling storms, the entire boundary current can reverse and flow to the west. We now examine the relationship of the winds to the transport timeseries. In general, currents over a shelf are seen to be most effectively driven by the wind component parallel to the coastline (Beardsley et al., 1985). We computed the coherence between the wind and the alongstream currents for different wind-component projections, and found that the maximum coherence across the array occurs for east-to-southeasterly/west-to-northwesterly winds. As a first-order comparison then, we chose to relate the transport timeseries with the wind component directed along the north Alaskan coastline (positive values point towards 105°T, in an oceanographic sense). The comparison between the along-coast winds and the Pacific water transport is shown in Fig. 15C. Overall, the two timeseries are significantly correlated ($r=0.59$). Visually, however, one can distinguish periods of enhanced and diminished correlation. To elucidate this we calculated the correlation coefficients as running means, over 5, 15 and 30 days, respectively. For the shorter running average the correlations were, at times, almost perfect. This occurs especially during the upwelling season (strong easterly winds, and westward transport in Fig. 15C), but there are also periods of strong westerly winds and increased eastward transport (i.e. downwelling conditions, for example in early October). Even the longer, and smoother, 30-day running average yields high correlations ($r>0.8$) for long periods of time (Fig. 15C; 5 and 15 days not shown).

The general trends in the wind-current correlation in Fig. 15C can be interpreted as follows. The two periods of high correlation

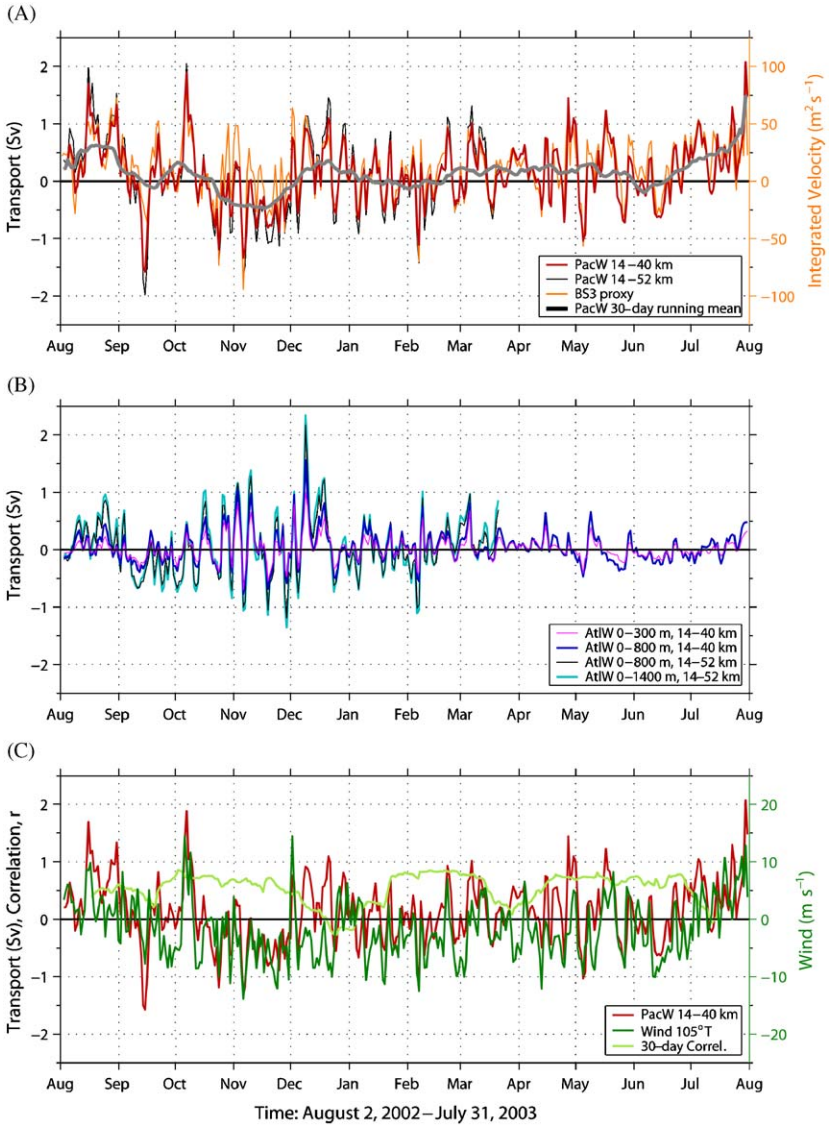

Fig. 15. Timeseries of daily transport calculated from the vertical sections for the domains given in the legends. Note that the timeseries for the larger domain (14–52 km), is shorter due to the truncated record of BS8 in March 2003. (A) Pacific water transport for two domains, superposed by the 30-day running average for the shorter domain. Also shown is the integrated velocity at BS3 (see right-hand scale); (B) Atlantic water transport for four different domains; (C) the Pacific water transport superposed by the along-coast (105°T) wind component measured at Pt. Barrow (right-hand scale), and the 30-day running correlation (r) between the two timeseries.

during October–November and February–March are largely due to upwelling storms. These two periods were characterized by strong flow reversals and enhanced upwelling of Atlantic water at the array site (Tsimitri and Pickart, 2006), which is seen in Fig. 10 (note the temporal distribution of realizations). Most of the upwelling events along the Beaufort slope seem to be caused by Pacific-born cyclones (Aleutian low systems) that veer northward toward the Bering Strait (Pickart and Moore, unpublished manuscript). During December–January, although there were numerous Aleutian low systems formed, most of them remained to the south due to a blocking high-pressure ridge over northern Alaska and the southern Arctic (Pickart and Moore, unpublished manuscript). Hence, even though increased winds may have been measured by the Pt. Barrow weather station, these were not canonical upwelling events in terms of the large-scale atmospheric conditions. (Ice cover may also have played a role, although ice was present in February–March as well when upwelling was strong.) This likely explains the low correlation in Fig. 15C during December–January. The other periods of low correlation in Fig. 15C are explainable by remote advective influences. In particular, the cold, winter-transformed Pacific water emanating from the Chukchi shelf arrived at the array site in late-March/early-April, associated with strong eastward flow over much of the array (Figs. 5 and 7A and B). And during the summer months, the eastward extension of the Alaskan Coastal Current brought a large quantity of warm Alaskan Coastal water (Figs. 5 and 7C and D). These upstream influences likely dominated any local wind effects.

6. Discussion

The results presented here have demonstrated that there is a narrow boundary current situated along the edge of the Beaufort shelf advecting Pacific-origin water to the east. There are three distinct seasonal configurations of the current, and synoptically the flow reverses to the west during upwelling storm events. Overall, these results were not unexpected: earlier studies have established the existence of this current, and synoptic transects farther to the west along the edge of the Chukchi shelf have

showed a similarly configured jet. However, the small mean volume transport of Pacific water over the year-long record came as a surprise. Part of the motivation for situating the array to the east of Pt. Barrow was that it would measure the cumulative transport of the three outflows from the Chukchi shelf—via Herald Canyon, the Central Channel, and Barrow Canyon. The expectation was that these outflows would be channeled by the bathymetry into an eastward-flowing shelfbreak jet carrying a significant fraction of the Bering Strait inflow towards the Canadian Arctic Archipelago and Fram Strait. Both the archipelago and Fram Strait are known to have a significant amount of Pacific water flowing through them (Taylor et al., 2003; Jones and Eert, 2006; Jones et al., 2008). Instead, according to our results, at least 70% of the Bering Strait inflow goes somewhere else.

The obvious question is, if the Pacific water inflow does not end up in the western Arctic boundary current, where does it go? One possibility is that some of it flows directly off the shelf as a well-defined current into the open Arctic. Such a pathway of Pacific water has been hypothesized based on temperature distributions in the Canadian Basin. Steele et al. (2004) present a schematic circulation scheme for the Chukchi/Bering summer water (their Fig. 9) in which the outflow from Herald Canyon extends offshore to join the transpolar drift, while the outflow from the Central Channel becomes entrained into the western limb of the Beaufort Gyre. This scheme is consistent with the fact that we saw very little of this water mass advected past our Beaufort slope array. However, it remains to be demonstrated how such a current can break the geostrophic constraint and flow off the shelf, especially since the Chukchi/Bering summer water is denser than the ambient water at the same depth in the basin interior and hence should feel the stretching effect of the bottom slope at the shelfbreak.

Another possible mechanism for transporting water offshore is via eddy formation. It is now established that the shelfbreak jet spawns eddies containing Pacific-origin water. This includes subsurface anti-cyclones containing winter-transformed water (Muench et al., 2000; Pickart et al., 2005; Mathis et al., 2007); subsurface (but shallower) anti-cyclones containing Chukchi/Bering summer water (R. Pickart, pers. comm., 2007); and surface-intensified anti-cyclones containing Alaskan Coastal water (Pickart et al., 2005). Based on the large number of eddies that populate the Canada Basin (Manley and Hunkins, 1985; Plueddemann and Krishfield, 2008), this would appear to be a dominant mechanism for off-shelf transport. However, the results of Spall et al. (2008) suggest that eddy formation due to hydrodynamic instability of the boundary current will result in property transport (e.g. temperature, potential vorticity) into the interior of the basin, but not significant mass transport. In other words, it results in an *exchange* of mass with the interior, with little net loss of transport from the boundary current. (Note that this could explain the temperature distribution of the Chukchi/Bering summer water described by Steele et al., 2004.)

A third possibility for the large disparity in transport between the Bering Strait inflow and the Beaufort slope boundary current is the effect of wind. As discussed above, the shelfbreak jet is highly sensitive to wind forcing, which often reverses the flow. In addition, less frequent downwelling storms (with westerly winds) enhance the eastward flow of the jet. Over the course of 2002–2003, the mean wind along 105°T at Pt. Barrow was 1.8 m s^{-1} out of the east. This means that, on average, the wind was opposing the topographically steered direction of the current, which presumably is reflected in the small mean transport measured at the array site. In an attempt to quantify this, a scatter plot of wind speed versus Pacific water transport was constructed (Fig. 16). As noted above, these two variables are significantly correlated (Fig. 15C). The scatter plot allows us to

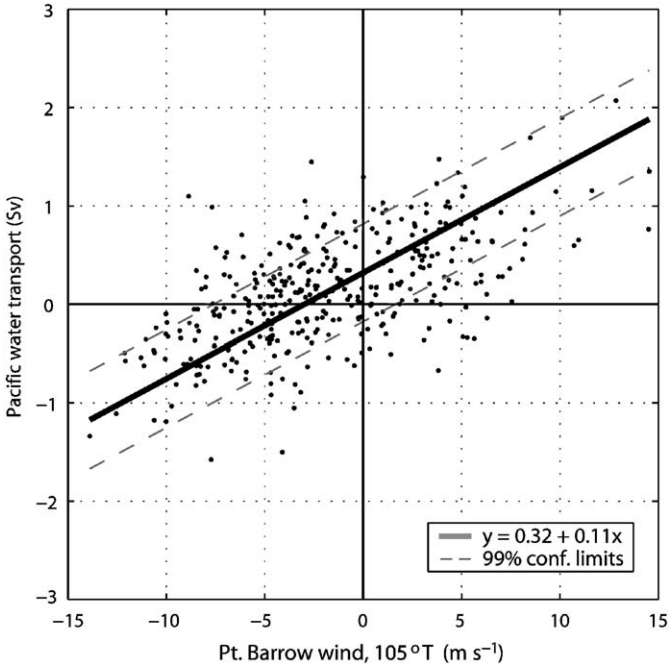

Fig. 16. Scatter plot of the Pacific water transport (14–40 km) and the along-coast (105°T) Pt. Barrow wind component (both shown in Fig. 15C). The solid line is the least-square regression line (see legend), and the dashed lines show the 99% confidence intervals.

evaluate the transport of the current at zero wind speed, which, according to the best-fit regression line in Fig. 16, is 0.32 Sv (versus 0.13 Sv measured). While the error bar for this calculation is large, it suggests that, when the wind is absent, a much greater percentage of the Bering Strait inflow ends up in the western Arctic boundary current. How might a succession of upwelling storms lead to the diminished measured transport? One possibility could be convergence of the alongslope flow (hence resulting in offshore mass flux) associated with the finite along-shelf length scale of the storms (for example, upwelling-favorable winds on one part of the slope and weak winds on another part of the slope). Another factor could be changes in orientation of the coastline (e.g. the sharp bend at Pt. Barrow). To answer this definitively, further work is required (likely using models).

Another aspect of wind forcing, which does not rely on coastal storm events, was addressed by Spall et al. (2008). When interior anti-cyclonic winds were added to their idealized model to produce the equivalent of the Beaufort Gyre, this, in conjunction with eddy formation, resulted in a significant mass flux from the boundary current into the interior. This suggests that a combination of hydrodynamic instability and winds, acting over the length of the Chukchi slope (and part of the Beaufort slope) could also be responsible for some of the loss of transport observed at our array.

It is well documented that the inflow through Bering Strait fluctuates on a variety of timescales, including strong seasonal variability. It is of interest, then, to see if there is any correlation between the flow through the strait and the transport of the boundary current at our array site. It is estimated that, in the mean, more than a third of the Bering Strait inflow makes its way through Barrow Canyon (T. Weingartner, pers. comm., 2007), and that during summer the Alaskan Coastal water takes about 2.5 months to travel from the strait to Barrow Canyon (Weingartner et al., 1998). We investigated this by using 12 months of velocity data from the near-bottom current meter record from mooring A3, just north of Bering Strait (Woodgate et al., 2005a). This record is considered to be a reasonable proxy for the net flow through the

strait (the 329°T-velocity may be converted to transport by applying a cross-sectional area of 3.9 km^2, see Fig. 5 in Woodgate et al., 2005a). Comparing the two daily transport series (and also weekly and monthly running averages) for time lags up to 6 months, we found no significant positive correlation. This result is perhaps not unexpected, based on our finding that such a large percentage of the inflow seems to go elsewhere besides the western Arctic Boundary current. The precise relationship between the Bering Strait transport and that of the western Arctic boundary current needs further consideration, including the role of the large-scale winds. In the future, by adding data from the second Beaufort slope deployment and also from the complimentary SBI mooring arrays on the Chukchi shelf/slope, our capacity to resolve the circulation patterns and timing of the Pacific water will be improved.

Acknowledgments

The authors are indebted to the following people: To John Kemp for preparing and deploying the moorings; to John Toole for helping with the ACM data processing; to Ryan Schrawder for turning around instrumentation for the array; to Rebecca Woodgate and Knut Aagaard for sharing the A3-mooring velocity data; to Tom Weingartner for many valuable discussions; to Paul Johnson and the Hawaii Mapping Research Group for constructing the composite bathymetric data set; and to Roger Goldsmith for assistance with numerous parts of the analysis. Lastly, we would like to acknowledge the hard work and expertise of Capt. David McKenzie and the crew of the USGS Polar Star for deploying the array, and Capt. Daniel Oliver and the crew of the USGS *Healy* for recovering the array. AN was funded by the Swedish Research Council; RP, PF, and DT were funded by Grant N00014-02-1-0317 of the Office of Naval Research.

References

Aagaard, K., 1984. The Beaufort Undercurrent. In: Barnes, P., Reimnitz, E. (Eds.), The Alaskan Beaufort Sea: Ecosystems and Environment. Academic Press, New York, pp. 47–71.

Aagaard, K., 1989. A synthesis of the Arctic Ocean circulation. Rapports et Procès-verbaux Reunion Conseil International pour l'Exploration de la Mer 188, 11–22.

Aagaard, K., Carmack, E.C., 1994. The Arctic Ocean and climate: a perspective. In: Johannessen, O.M., Muench, R.D., Overland, J.E. (Eds.), The Polar Oceans and their Role in Shaping the Global Environment. Geophysical Monograph, vol. 85. American Geophysical Union, Washington DC, pp. 5–20.

Beardsley, R.C., Chapman, D.C., Brink, K.H., Ramp, S.R., Schlitz, R., 1985. The Nantucket Shoals Flix Experiment (NSFE79). Journal of Physical Oceanography 15, 713–748.

Coachman, L.K., Aagaard, K., Tripp, R.B., 1975. Bering Strait: the Regional Physical Oceanography. University of Washington Press, Seattle.

D'Asaro, E.A., 1988. Observations of small eddies in the Beaufort Sea. Journal of Geophysical Research 93, 6669–6684.

Dmitrenko, I.A., Polyakov, I.V., Kirillov, S.A., Timokhov, L.A., Simmons, H.L., Ivanov, V.V., Walsh, D., 2006. Seasonal variability of Atlantic water on the continental slope of the Laptev Sea during 2002–2004. Earth and Planetary Science Letters 244, 735–743.

Doherty, K.W., Frye, D.E., Liberatore, S.P., Toole, J.M., 1999. A moored profiling instrument. Journal of Atmospheric and Oceanic Technology 16, 1816–1829.

Fratantoni, P.S., Zimmerman, S., Pickart, R.S., Swartz, M., 2006. Western Arctic Shelf-Basin Interactions Experiment: Processing and calibration of moored profiler data form the Beaufort shelf-edge mooring array. Woods Hole Oceanographic Institution Technical Report WHOI-2006-15, Woods Hole, MA, 34pp.

Garrison, G.R., Becker, P., 1976. The Barrow submarine canyon: a drain for the Chukchi Sea. Journal of Geophysical Research 81, 4445–4453.

Grebmeier, J.M., Harvey, H.R. (Eds.), 2005. The Western Arctic Shelf-Basin Interactions (SBI) Project: An overview (Editorial), Deep Sea Research II 52, 3109–3115.

Johnson, P.D., Edwards, M.H., Wright, D., 2006. Data processing, visualization and distribution for support of science programs in the Arctic Ocean, EOS Transactions AGU, 87(52) (Fall Meeting Supplement, Abstract IN41A-0875).

Jones, E.P., Eert, A.J., 2006. Waters of Nares Strait in 2001. Polarforschung 74, 185–189.

Jones, E.P., Swift, J.H., Anderson, L.G., Lipizer, M., Civitarese, G., Falkner, K.K., Kattner, G., McLaughlin, F., 2003. Tracing Pacific water in the North Atlantic Ocean. Journal of Geophysical Research 108.

Jones, E.P., Anderson, L.G., Jutterström, S., Swift, J.H., 2008. Sources and distribution of fresh water in the East Greenland Current. Progress in Oceanography 78 (1), 37–44.

Kadko, D., Muench, R., 2005. Evaluation of shelf-basin interaction in the western Arctic by use of short-lived radium isotopes: the importance of mesoscale processes. Deep-Sea Research II 52, 3227–3244.

Karcher, M.J., Oberhuber, J.M., 2002. Pathways and modification of the upper and intermediate waters of the Arctic Ocean. Journal of Geophysical Research 107.

Karcher, M., Kauker, F., Gerdes, R., Hunke, E., Zhang, J., 2007. On the dynamics of Atlantic water circulation in the Arctic Ocean. Journal of Geophysical Research 112.

Kikuchi, T., Inoue, J., Morrison, J.H., 2005. Temperature difference across the Lomonosov Ridge: implications for the Atlantic water circulation in the Arctic Ocean. Geophysical Research Letters 32.

Llinas, L., Pickart, R.S., Mathis, J.T., Smith, S.L., 2008. Zooplankton inside an Arctic Ocean cold-core eddy: Probable origin and fate. Deep-Sea Research II, this issue [doi:10.1016/j.dsr2.2008.10.020].

Loeng, H., Ozhigin, V., Adlandsvsk, B., Sagen, H., 1993. Current measurements in the north eastern Barents Sea. In: Proceedings of the ICES Statutory Meeting 1993.

Manley, T.O., Hunkins, K., 1985. Mesoscale eddies of the Arctic Ocean. Journal of Geophysical Research 90, 4911–4930.

Maslowski, W., Marble, E., Walczowski, W., Schauer, U., Clement, J.L., Semtner, J.J., 2004. On climatological mass, heat, and salt transport through the Barents Sea and Fram Strait from a pan-Arctic coupled ice-ocean model simulation. Journal of Geophysical Research 109, C03032.

Mathis, J.T., Pickart, R.S., Hansell, D.A., Kadko, D., Bates, N.R., 2007. Eddy transport of organic carbon and nutrients from the Chukchi shelf into the deep Arctic Basin. Journal of Geophysical Research 112.

Melling, H., 1993. The formation of a haline shelf front in wintertime in an ice-covered arctic sea. Continental Shelf Research 13, 1123–1147.

Mountain, D.G., Coachman, L.K., Aagaard, K., 1976. On the flow through Barrow Canyon. Journal of Physical Oceanography 6, 461–470.

Muench, R.D., Schumacher, J.D., Salo, S.A., 1988. Winter currents and hydrographic conditions on the northern central Bering Sea shelf. Journal of Geophysical Research 93, 516–526.

Muench, R.D., Gunn, J.T., Whitledge, T.E., Schlosser, P., Smethie Jr., W., 2000. An Arctic Ocean cold core eddy. Journal of Geophysical Research 105, 23997–24006.

Münchow, A., Carmack, E.C., 1997. Synoptic flow and density observations near an Arctic shelf break. Journal of Physical Oceanography 27, 1402–1419.

Münchow, A., Pickart, R.S., Weingartner, T.J., Woodgate, R.A., Kadko, D., 2006. Arctic boundary currents over the Chukchi and Beaufort slope seas: Observational snapshots, transports, scales, and spatial variability from ADCP surveys. EOS Transactions AGU 87(36) (Ocean Sciences Meeting Supplement, Abstract OS33N-03).

Newton, J.L., Coachman, L.K., 1974. Atlantic water circulation in the Canada Basin. Arctic 27, 297–303.

Pickart, R.S., 2004. Shelfbreak circulation in the Alaskan Beaufort Sea: mean structure and variability. Journal of Geophysical Research 109, C04024.

Pickart, R.S., McKee, T.K., Torres, D.J., Harrington, S.A., 1999. Mean structure and interannual variability of the slopewater system south of Newfoundland. Journal of Physical Oceanography 29, 2541–2558.

Pickart, R.S., Weingartner, T.J., Pratt, L.J., Zimmermann, S., Torres, D.J., 2005. Flow of winter-transformed Pacific water into the western Arctic. Deep-Sea Research II 52, 3175–3198.

Pickart, R.S., Fratantoni, P.S., Goldsmith, R.A., Moore, G.W.K., Agnew, T., Vandeweghe, J., 2006. Upwelling in the western Arctic boundary current north of Alaska. EOS Transactions AGU 87 (36) (Ocean Sciences Meeting Supplement, Abstract OS350-07).

Pickart, R.S., Pratt, L.J., Torres, D.J., Whitledge, T.E., Proshutinsky, A.Y., Aagaard, K., Agnew, T.A., Moore, G.W.K., Dail, H.J., 2009a. Evolution and dynamics of the flow through Herald Canyon in the Western Chukchi Sea. Deep-Sea Research II, accepted.

Pickart, R.S., Moore, G.W.K., Macdonald, A.M., Renfrew, I.A., Walsh, J.E., Kessler, W.S., 2009b. Seasonal evolution of Aleutian low-pressure systems: Implications for the North Pacific sub-polar circulation. Journal of Physical Oceanography, accepted.

Plueddemann, A.J., Krishfield, R., 2008. Physical properties of eddies in the western Arctic. Journal of Geophysical Research, submitted for publication.

Proshutinsky, A.Y., Johnson, M.A., 1997. Two circulation regimes of the wind-driven Arctic Ocean. Journal of Geophysical Research 102, 12493–12514.

Proshutinsky, A., Yang, J., Krishfield, R., Gerdes., R., Karcher, M., Kauker, F., Koeberle, C., Hakkinen, S., Hibler, W., Holland, D., Maqueda, M., Holloway, G., Hunke, E., Maslowski, W., Steele, M., Zhang, J., 2005. Arctic Ocean Study: Synthesis of model results and observations. EOS Transactions AGU 86 (40), 368.

Roach, A.T., Aagaard, K., Pease, C.H., Salo, S.A., Weingartner, T., Pavlov, V., Kulakov, M., 1995. Direct measurements of transport ans water properties through the Bering Strait. Journal of Geophysical Research 100, 18443–18457.

Rudels, B., Jones, E.P., Anderson, L.G., Kattner, G., 1994. On the intermediate depth waters of the Arctic Ocean. In: Johannessen, O.M., Muench, R.D., Overland, J.E. (Eds.), The Polar Oceans and their Role in Shaping the Global Environment, Geophysical Monograph, vol. 85. American Geophysical Union, Washington DC, pp. 33–46.

Rudels, B., Jones, E.P., Schauer, U., Eriksson, P., 2004. Atlantic sources of the Arctic Ocean surface and halocline waters. Polar Research 23, 181–208.

Schauer, U., Muench, R.D., Rudels, B., Timokhov, L., 1997. Impact of eastern Arctic shelf waters on the Nansen Basin intermediate layers. Journal of Geophysical Research 102, 3371–3382.

Schauer, U., Rudels, B., Jones, E.P., Anderson, L.G., Muench, R.D., Björk, G., Swift, J.H., Ivanov, V., Larsson, A.-M., 2002a. Confluence and redistribution of Atlantic water in the Nansen, Amundsen and Makarov basins. Annales Geophysicae, European Geophysical Society 20, 257–273.

Schauer, U., Loeng, H., Rudels, B., Ozhigin, V.K., Dieck, W., 2002b. Atlantic water flow through the Barents and Kara Seas. Deep-Sea Research I 49, 2281–2298.

Schauer, U., Fahrbach, E., Osterhus, S., Rohardt, G., 2004. Arctic warming through the Fram Strait: Oceanic heat transport from 3 years of measurements. Journal of Geophysical Research 109.

Shimada, K., Carmack, E.C., Hatakeyama, K., Takizawa, T., 2001. Varieties of shallow temperature maximum waters in the western Canadian Basin of the Arctic Ocean. Geophysical Research Letters 28, 3441–3444.

Shimada, K., McLaughlin, F., Carmack, E., Proshutinsky, A., Nishino, S., Itoh, M., 2004. Penetration of the 1990s warm temperature anomaly of Atlantic water in the Canada Basin. Geophysical Research Letters 31.

Smethie Jr., W.M., Schlosser, P., Bönisch, G., 2000. Renewal and circulation of intermediate waters in the Canadian Basin observed on the SCICEX 96 cruise. Journal of Geophysical Research 105, 1105–1121.

Spall, M.A., 2007. Circulation and water mass transformation in a model of the Chukchi Sea. Journal of Geophysical Research 112.

Spall, M.A., Pickart, R.S., Fratantoni, P.S., Plueddemann, A.J., 2008. Western Arctic shelfbreak eddies: Formation and transport. Journal of Physical Oceanography 38, 1644–1668.

Steele, M., Morison, J., Ermold, W., Rigor, I., Ortmeyer, M., Shimada, K., 2004. Circulation of summer Pacific halocline water in the Arctic Ocean. Journal of Geophysical Research 109, C02027.

Taylor, J.R., Falkner, K.K., Schauer, U., Meredith, M., 2003. Quantitative considerations of dissolved barium as a tracer in the Arctic Ocean. Journal of Geophysical Research 108.

Tsimitri, C., Pickart, R.S., 2006. Characterizing upwelling events in the western Arctic. EOS Transaction AGU 87 (36) (Ocean Sciences Meeting Supplement, Abstract OS350-08).

Våge, K., Pickart, R.S., Moore, G.W.K., Ribergaard, M.H., 2008. Winter mixed-layer development in the central Irminger Sea: The effect of strong, intermittent wind events. Journal of Physical Oceanography 38, 541–565.

Weingartner, T.J., Cavalieri, D.J., Aagaard, K., Sasaki, Y., 1998. Circulation, dense water formation, and outflow on the northeast Chukchi shelf. Journal of Geophysical Research 103, 7647–7661.

Weingartner, T., Aagaard, K., Woodgate, R., Danielson, S., Sasaki, Y., Cavalieri, D., 2005. Circulation on the north central Chukchi Sea shelf. Deep-Sea Research II 52, 3150–3174.

Whitledge, T.E., 2006. Russian-American long term census of the Arctic (RUSALCA): Nutrient, pigment and productivity dynamics in US and Russian waters of the Chukchi Sea. EOS Transactions AGU 87 (36) (Ocean Sciences Meeting Supplement, Abstract OS43N-01).

Winsor, P., Chapman, D.C., 2004. Pathways of Pacific water across the Chukchi Sea: a numerical model study. Journal of Geophysical Research 109, C03002.

Woodgate, R.A., Aagaard, K., Muench, R.D., Gunn, J., Björk, G., Rudels, B., Roach, A.T., Schauer, U., 2001. The Arctic Ocean boundary current along the Eurasian slope and the adjacent Lomonosov Ridge: water mass properties, transports and transformations from moored instruments. Deep-Sea Research I 48, 1757–1792.

Woodgate, R.A., Aagaard, K., Weingartner, T.J., 2005a. Monthly temperature, salinity, and transport variability of the Bering Strait through flow. Geophysical Research Letters 32, L04601.

Woodgate, R.A., Aagaard, K., Weingartner, T.J., 2005b. A year in the physical oceanography of the Chukchi Sea: moored measurements from autumn 1990–1991. Deep-Sea Research II 52, 3116–3149.